THE UNIVERSITY OF CALGARY

Control of Oscillatory Discharge in an Electrosensory Neuron

by

Neal Allen Scott Lemon

A THESIS
SUBMITTED TO THE FACULTY OF GRADUATE STUDIES
IN PARTIAL FULFILMENT OF THE REQUIREMENTS FOR THE
DEGREE OF MASTER OF SCIENCE

DEPARTMENT OF NEUROSCIENCE

CALGARY, ALBERTA
DECEMBER, 1999

ABSTRACT

Backpropagating dendritic Na^+ spikes generate a depolarizing afterpotential (DAP) at the soma of pyramidal cells in the electrosensory lateral line lobe (ELL) of weakly electric fish. During repetitive discharge the DAP contributes to the generation of oscillatory spike bursts. The present study examined the soma-dendritic interactions that regulate the DAP and burst generation. Intracellular recordings were obtained from ELL pyramidal somata and apical dendrites in an *in vitro* slice preparation. Spike output exhibited a voltage- or time-dependent shift from tonic to burst discharge when interspike intervals fell within ~3 - 7 ms. Oscillatory spike bursts consisted of 2 - 7 spikes which were terminated by a high frequency somatic spike doublet and burst AHP. The primary factor controlling burst frequency was the rate of membrane depolarization during a burst, as determined by the balance between somatic AHPs and the DAP. Local dendritic TTX ejection prevented spike backpropagation and isolated somatic AHPs, revealing that AHPs were stable during repetitive discharge. In contrast, a frequency-dependent broadening and summation of dendritic spikes at interspike intervals of ~3 - 7 ms enhanced the somatic DAP. The short interspike interval of the somatic spike doublet fell within the dendritic refractory period, preventing backpropagation of the second spike of the doublet. The sudden failure of backpropagation during a burst truncated the dendritic depolarization and removed the somatic DAP, uncovering the burst AHP. These data reveal a novel soma-dendritic interaction that allows conditional backpropagation to control the generation, threshold, and frequency of oscillatory spike bursts.

ACKNOWLEDGEMENTS

I have been blessed to work with Drs. Ray W. Turner and Ezequiel Morales over the past two years. Dr. Turner has provided me with exceptional intellectual guidance and supervision which will not be forgotten. I deeply appreciate the friendly learning environment which Drs. Turner and Morales fostered. I also wish to thank my supervisory committee, Drs Quentin Pittman and Brian MacVicar. I would also like to thank Dr. C.W. Teskey for serving as a member of my examining committee. Finally, I acknowledge financial support from the Medical Research Council of Canada (MRC) and the University of Calgary.

This thesis is dedicated to my parents, Allen and Lois Lemon. Their love and support is deeply appreciated.

TABLE OF CONTENTS

LIST OF TABLES

LIST OF FIGURES

LIST OF ABBREVIATIONS

A	amplitude
ACSF	artificial cerebrospinal fluid
AM	amplitude modulation
BAHP	burst afterhyperpolarization
CLS	centrolateral segment
CMS	centromedial segment
C-T	condition-test
DAP	depolarizing afterpotential
DC	direct current
ELL	electrosensory lateral line lobe
EOD	eletric organ discharge
fAHP	fast afterhyperpolarization
ISI	interspike interval
LS	lateral segment
m	slope
MS	medial segment
PCL	pyramidal cell layer
Ri	input resistance
RMP	resting membrane potential
sAHP	slow afterhyperpolarization
TEA	Tetraethyl ammonium chloride
TTX	Tetrodotoxin

CHAPTER 1

INTRODUCTION

ELECTRORECEPTION

Many aquatic animals have the ability to passively sense very weak electric fields using electroreceptors (Moller, 1995). For instance, freshwater catfish respond to electric field gradients as low as 1 μV per centimeter. This high sensitivity enables electrosensitive animals to locate prey using the weak electric fields emitted into the surrounding water during physiological muscle contractions (ie. gill movements). A subset of fish in addition to having an electrosensory system possess electric organs. These weakly electric fish generate electric fields which they use for the active detection of objects and for communication (for review, see Heiligenberg, 1991; Bastian, 1994). One such weakly electric fish is the Brown Ghost Knife fish (*Apteronotus leptorhynchus*) which both produces and senses its own weakly electric organ discharge (EOD). This EOD is continously generated as a sinusoidal waveform in the millivolt range. The Brown Ghost Knife fish has two types of electroreceptors distributed over its body surface. The T-type electroreceptor encodes changes in EOD signal phase, while the P-type electroreceptor senses changes in EOD amplitude induced by objects in the surrounding environment. The electrosensory system uses this information to compare differential phase and amplitude modulations of the EOD over the body surface to determine the physical location of objects, a process termed electrolocation.

ELECTROSENSORY LATERAL LINE LOBE (ELL)

Afferents of these electroreceptors project to the ELL, a medullary nucleus where they synapse on basilar dendrites of granule cells and pyramidal cells. The pyramidal cells are the primary output cells of the ELL. Pyramidal cells are confined to a well defined pyramidal cell layer (PCL), and project an apical dendritic tree 600-800 μm into an overlying molecular layer. The PCL extends across four topographic maps positioned side-by-side in the medio-lateral plane, the medial segment (MS), centromedial segment (CMS), centrolateral segment (CLS) and lateral segment (LS) (Maler, 1979) (Fig. 1). The outer three maps (CMS, CLS, and LS) receive identical primary afferent input from the P-type electroreceptors involved in encoding changes in the magnitude and frequency of amplitude modulations (AM) of external fields.

Shumway (1989) investigated the response of ELL pyramidal cells across the segmental maps *in vivo* to varying AM frequencies in an externally applied field and found several differences in cell responsiveness. Pyramidal units in the lateral segment (LS) were found to have larger receptive fields which were more sensitive than those in the CMS to step changes in electric field amplitude. The LS units also responded more phasically and with shorter latencies to step changes in electric field amplitude. The strength of the inhibitory surround in the center-surround receptive field was weakest in the LS and strongest in the CMS. The majority of units in the LS responded preferentially to high frequency AMs compared to the CMS units which responded preferentially to low frequency AMs. Specifically, CMS pyramidal cells responded best to AM frequencies of ~1-10 Hz, CLS cells to ~20-35 Hz, and LS cells to ~50-120 Hz (Fig. 2*A-C*). These differences led Shumway to postulate that the ELL maps may be the place where

temporal and spatial sensory information begins to be processed separately. Shumway believed that the CMS map could provide high spatial but poor temporal resolution. The LS in turn would provide lower spatial contrast with higher temporal resolution.

More recent recordings in ELL slices *in vitro* revealed the presence of oscillatory burst discharge in ELL pyramidal cells and its associated circuitry (Mathieson and Maler, 1988; Turner et al., 1994, 1996). Importantly, the nature of these bursts shift across the segmental maps in a manner consistent with the frequency selectivity of pyramidal cells *in vivo* (Turner et al., 1996)(Fig. 2*B*). This led to the proposal that oscillatory discharge inherent to the ELL may be the cellular basis for frequency selectivity of pyramidal cells across the segmental maps *in vivo* (Turner et al., 1994).

BURST DISCHARGE IN ELL PYRAMIDAL CELLS

In vitro recordings have revealed the presence of both a slow and fast form of oscillatory burst discharge in pyramidal cells (Fig. 1). The slow form of spike burst is generated at a rate of ~0.3–3Hz and is driven by slow depolarizing shifts in membrane potential. It was found that several characteristics of slow oscillatory spike bursts changed significantly from the CMS to the LS. These changes included a reduction in oscillatory period (Fig. 2*D*), shorter burst duration (Fig. 2*E*), as well as a decrease in the number of spikes/burst (Fig. 2*F*)(Turner et al., 1996). There was also an increase in spike frequency within bursts from the CMS to the LS (Turner et al., 1996). The second form of oscillatory spike burst is generated at 15-200 Hz by way of a novel mechanism involving the backpropagation of dendritic spikes (Turner et al., 1994). Turner et al. noted that each spike burst was terminated by a bAHP that was generated in relation to a preceding high frequency spike doublet. It is presently unknown whether fast oscillatory bursts exhibit a

similar pattern of change to those reported for slow oscillatory bursts across segmental maps (Fig. 2). It is known however that these fast oscillatory bursts play a role in feature extraction *in vivo* (Gabianni et al., 1996). One intent of this project is to more carefully determine the properties and mechanisms underlying the fast oscillatory bursts in the CMS map, with the long term objective of comparing the properties of fast oscillatory bursts across the ELL maps.

Figure 1.

On the left is a cresyl-violet stained transverse section at the medullary level of *A.leptorhynchus*, showing the boundaries between four segmental maps of the ELL (MS, CMS, CLS, LS). The clear laminae of the pyramidal cell layer (PCL) and granule cell layer (GCL) are indicated. On the right are representative examples of spontaneous burst activity in pyramidal cells recorded in the CMS and LS segmental maps. *A*, *B*, Pyramidal cells in both segments can exhibit slow spontaneous oscillatory shifts in membrane potential that generate spike bursts. Note the longer duration of spike bursts in CMS cells (*A*) compared to LS cells (*B*). The period of spike bursts was 2.5 s in *A* and 0.58 s in *B*. *C*, *D*, Expanded traces of spike discharge over the regions indicated in *A* and *B* reveal a second, faster form of repetitive spike bursts in both CMS and LS cells. Small arrows (*C, D)* indicate timing of bAHPs that terminate each spike burst (Turner et al. 1994). The period of spike bursts was 0.02s in C and D. The calibration bar (mV) in *D* also applies to *A-C*. Abbreviations: ELL, electrosensory lateral line lobe; PCL, pyramidal cell layer; GCL, granule cell layer; MS, medial segment; CMS, centromedial segment; CLS, centrolateral segment; LS, lateral segment. Figure has been modified from Turner et al. (1996).

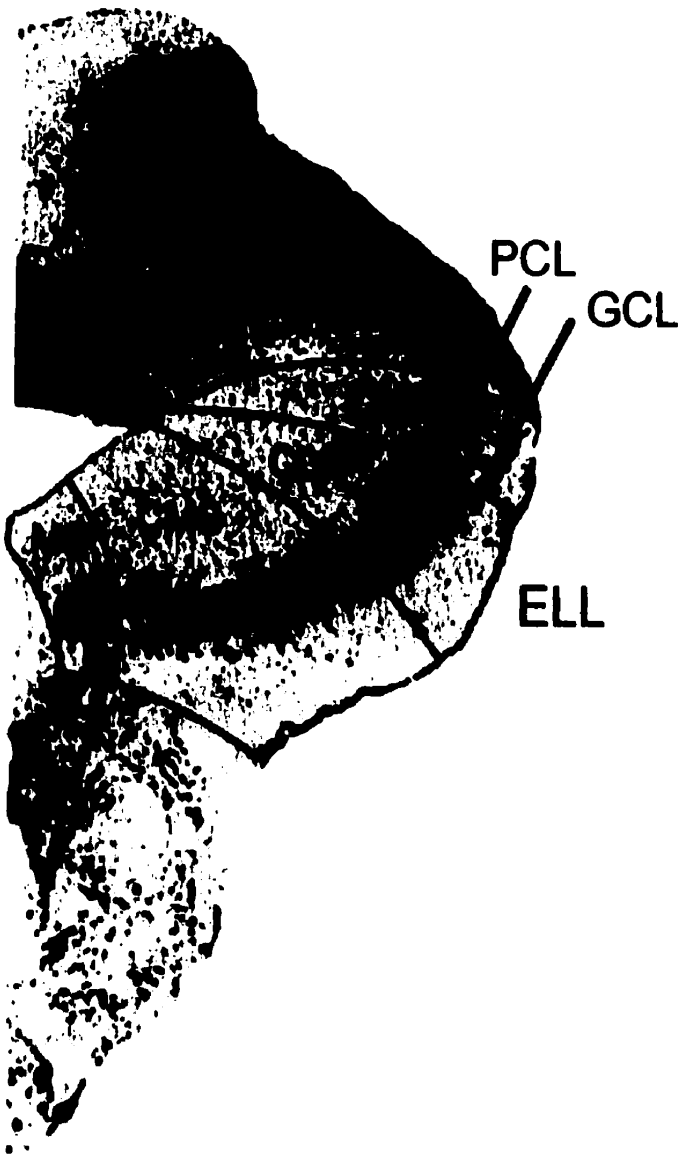
PCL
GCL
ELL

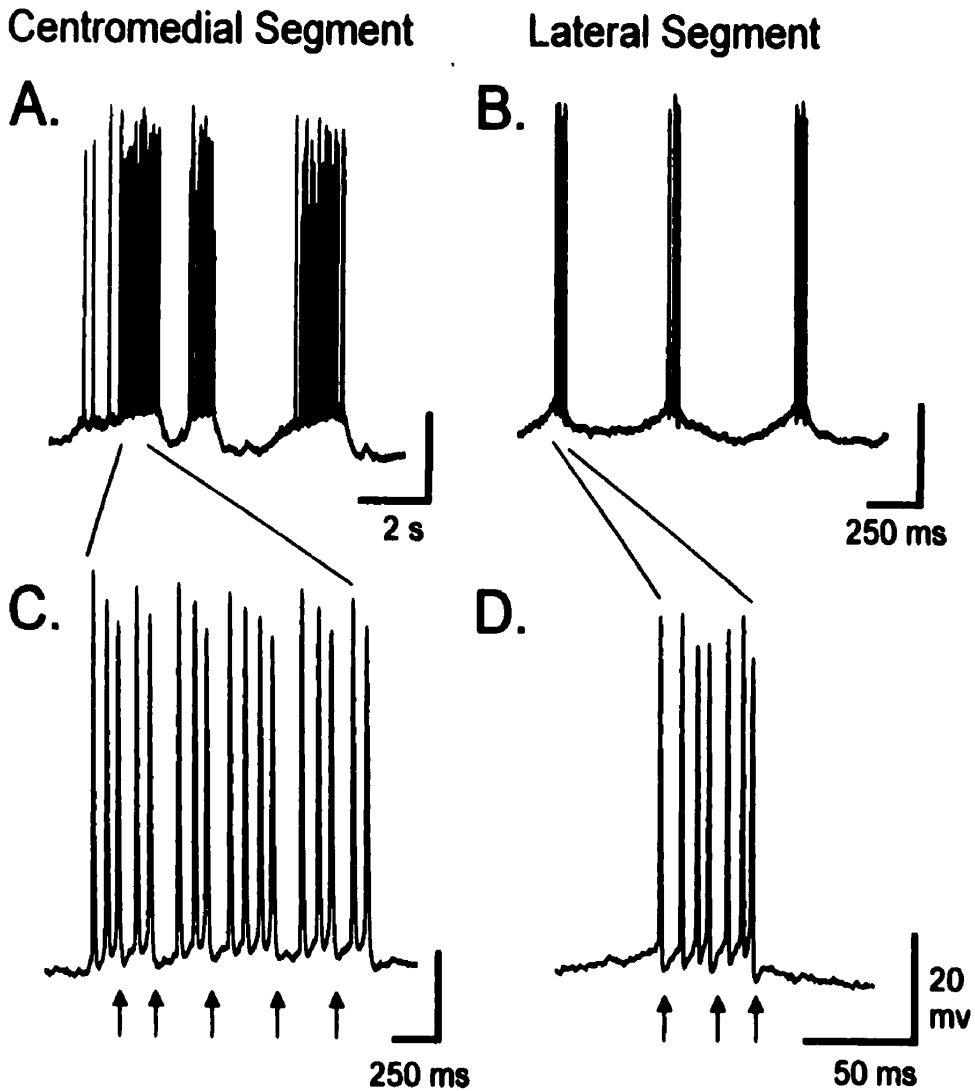
Centromedial Segment
Lateral Segment
A.
B.
2 s
250 ms
C.
D.
250 ms
20
mv
50 ms

Figure 2.

The nature of burst discharge *in vitro* shifts across segmental maps in a manner consistent with pyramidal cell frequency selectivity *in vivo*. *A-C*, Pyramidal units in the LS respond with a maximal firing response to higher frequencies of AM, while pyramidal units in the CMS produce a maximal response to lower frequencies of AM *in vivo*. Specifically CMS cells responded best to AM frequencies of ~1-10 Hz (*A*), CLS cells to frequencies of ~20-35 Hz (*B*), and LS cells to frequencies of ~ 50-120 Hz (*C*)(modified from Shumway, 1989). *D-F*, Several characteristics of slow oscillatory spike bursts *in vitro* change significantly from the CMS to LS. These changes include a reduction in oscillation period (*D*), shorter burst duration (*E*), as well as a decrease in the number of spikes/burst (F) (modified from Turner et al. 1996).

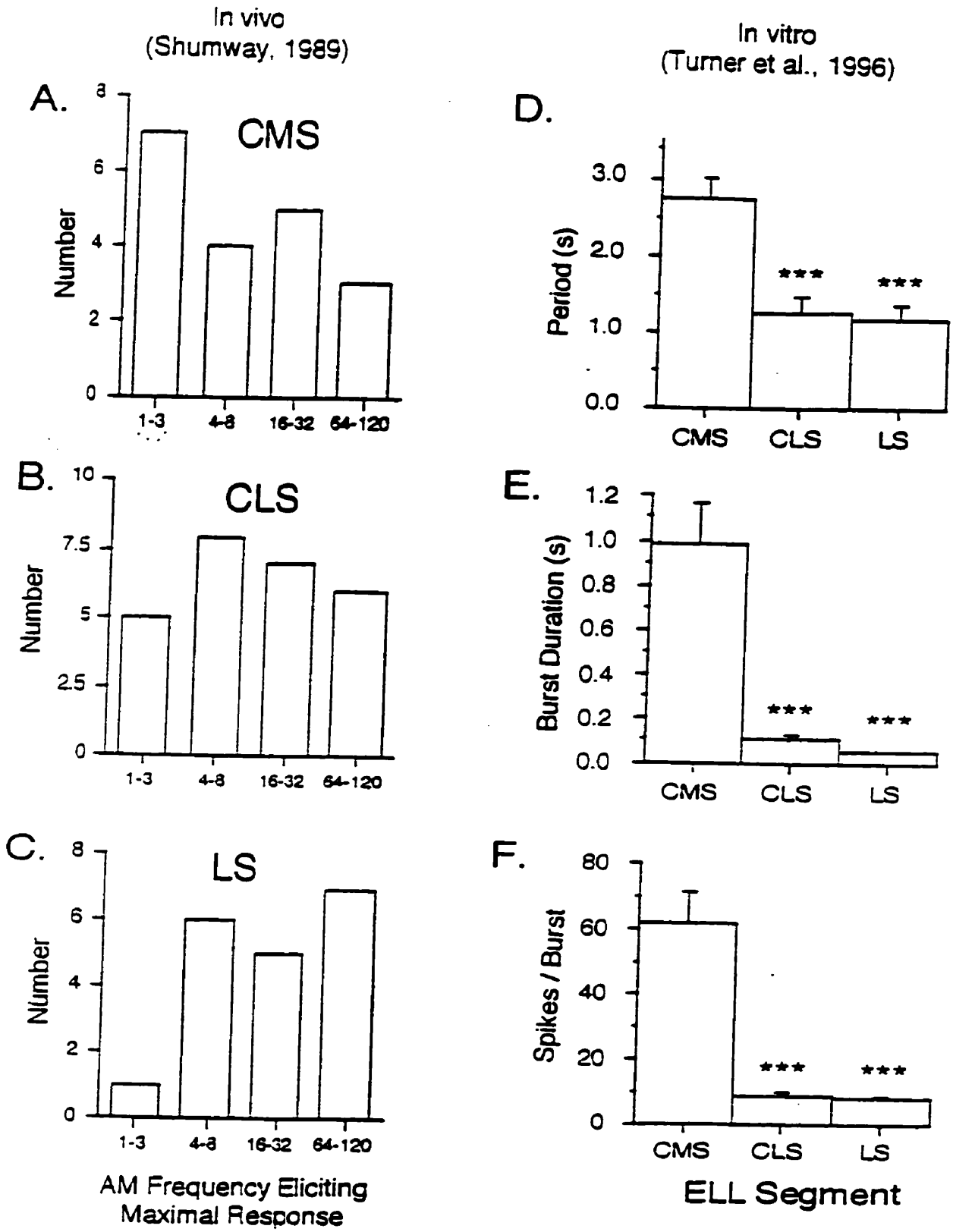
In vivo
(Shumway, 1989)
In vitro
(Turner et al., 1996)
A.
CMS
Number
0
2
4
6
8
1-3
4-8
16-32
64-120
B.
CLS
Number
0
2.5
5
7.5
10
1-3
4-8
16-32
64-120
C.
LS
Number
0
2
4
6
8
1-3
4-8
16-32
64-120
AM Frequency Eliciting
Maximal Response
D.
Period (s)
0.0
1.0
2.0
3.0
***
***
CMS
CLS
LS
E.
Burst Duration (s)
0.0
0.2
0.4
0.6
0.8
1.0
1.2
***
***
CMS
CLS
LS
F.
Spikes / Burst
0
20
40
60
80
***
***
CMS
CLS
LS
ELL Segment

SPIKE BACKPROPAGATION

Turner et al. (1994) established that the active properties of dendrites in pyramidal cells were key to the generation of spike bursts. The concept of active dendritic membranes and Na^+ spike invasion of the dendritic tree has been recognized for some time. Cragg and Hamlyn (1955) first recorded at the field potential level that antidromic or orthodromic stimulation evoked a short-duration, negative field potential that conducted over the somatodendritic axis of CA1 hipoocampal pyramidal cells *in vivo*. Spencer and Kandel's (1961) model for dendritic spike generation proposed that synaptic depolarization leads to the initial activation of a spike from dendritic membrane "hot spots", local regions exhibiting a low threshold for action potential initiation. Dendritic membranes of many neurons contain a sufficient density of Na^+ channels to generate active Na^+ spike discharge (Johnston et al., 1996, Mainen et al., 1995, Yuste, 1996). However, the soma typically has the lowest threshold for generating a spike. Membrane depolarizations therefore usually initiate spike discharge at the soma (Richardson et al., 1987; Turner et al., 1991; Spruston et al., 1995; Stuart and Sakmann, 1994). In hippocampal pyramidal cell dendrites the density of Na^+ channels is constant even up to 350 μM from the soma (Johnston et al., 1996). This allows spikes to retrogradely conduct from the soma and out through the dendritic tree in a process termed "spike backpropagation". It is now well established that antidromic Na^+ dependent action potentials propagate over ~ 2/3 of the axis of hippocampal pyramidal neuron dendrites (Miyakawa and Kato,1986; Richardson et al., 1987; Turner et al., 1991).

Spruston et al. (1995) demonstrated that single action potentials can invade the distal dendrites of CA1 neurons and result in substantial elevations of $[Ca^{2+}]_i$. This

finding suggested that active backpropagation of action potentials is supported by voltage-gated Na+ channels distributed over the entire apical dendrite. During trains of action potentials there is a frequency dependent decrease in the amplitude of action potentials in CA1 neuron dendrites. The amplitude decrease has been accounted for by a cumulative inactivation of dendritic Na^+ channels (Mickus et al. 1999; Colbert et al. 1997; Fleidervish et al. 1996). A decrease in dendritic spike amplitude with distance from the soma is due to the action of Kv4.2 (A-type) K^+ channels that increase in density from soma to distal regions of dendrites (Hoffman et al. 1997; Hoffman and Johnston, 1998). Modeling studies show that even a 5 mV shift in the Kv4.2 channel's activation curve can increase action potential amplitude in CA1 dendrites (Hoffman and Johnston, 1999). This shift in the activation curve can be achieved by the downregulation of A-channels by protein kinase activation (Hoffman and Johnston, 1999). These authors hypothesize that Na^+ channel inactivation or K^+ channel activation during action potential trains allows only the first few spikes in a train to actively propagate the entire extent of the dendrites.

During trains of action potentials there is a differential increase in $[Ca^{2+}]_i$ across the neuron. The rise in $[Ca^{2+}]_i$ is small in the soma, highest in proximal apical dendrites and basal dendrites and small again in the distal apical dendrites (Johnston et al. 1996). Broadening of action potentials by the addition of TEA makes the rise in $[Ca^{2+}]_i$ more uniform, with large increases in both proximal and distal dendrites. Imaging with a Na^+ sensitive dye by Jaffe et al. (1992) suggested that the influx of Ca^{2+} into the dendrites is driven by Na^+ dependent action potentials. Both high-voltage and low-voltage activated Ca^{2+} channels open during backpropagating action potentials and can further generate

dendritic Ca^{2+} spikes under conditions of K^+ channel blockade (Magee and Carruth, 1999; Golding et al., 1999).

Recent work has begun to identify the functional significance of backpropagation. Backpropagating spikes have been shown to trigger a dendritic Ca^{2+} influx which can regulate synaptic plasticity or enhance dendrite-soma coupling (Spruston et al., 1995; Callaway and Ross 1995; Markram et al., 1997; Magee and Johnston, 1997; Magee et al., 1998; Larkum et al., 1999). The occurrence of backpropagating spikes in olfactory mitral cells implicates their role in presynaptic dendritic transmitter release (Chen et al., 1997; Bischofberger and Jones, 1997).

Turner et al. (1994) first reported that backpropagating spikes also contribute to the generation of oscillatory discharge in ELL pyramidal cells. In particular, Na^+ spikes were reported to backpropagate into apical dendrites to drive somatic depolarizations. This represents a new and important addition to our understanding of the functional role of backpropagating spikes. Moreover, comparison of the basic properties of burst discharge in pyramidal cells suggests that this mechanism is likely active in several different cell types (Calvin and Seypert 1976; Calvin and Hartline, 1977; Granit et al., 1963; Nelson and Burke, 1967; Mainen and Sejnowski, 1996; Gray and McCormick, 1996, Wang, 1999).

SPIKE DISCHARGE IN ELL PYRAMIDAL NEURONS

In ELL pyramidal cells spike initiation is near the soma with spikes backpropagating over at least the initial 200 μm of apical dendrites. Spike discharge recorded in either pyramidal cell somata or apical dendrites in response to current injection is thus initiated at the soma, followed by backpropagation into apical dendrites (Fig.3 *A,B*).

Near threshold for spike discharge, pyramidal cells generate TTX-sensitive spikes, with the frequency of spikes increasing during membrane depolarization. Spikes recorded in somatic membrane are much shorter in duration and larger in amplitude than those recorded in dendrites (Table 1). Immediately following a somatic spike there is a fast afterhyperpolarization (fAHP). After the fAHP there is a depolarizing afterpotential (DAP) which is followed by a slower afterhyperpolarization (sAHP)(Fig. 3*A*,*C*). In contrast, only a sAHP is recorded in dendritic membrane (Fig. 3*B*).

Superimposing antidromic spikes recorded in somatic and dendritic locations indicates that the dendritic spike is of similar duration to the somatic DAP (Turner et al., 1994) (Fig. 3*C*). These authors in fact established a direct relationship between dendritic spike discharge and the somatic DAP using focal TTX ejections in the dendritic region.

Spike afterpotentials are important to the underlying mechanism for burst discharge. An expanded view of an oscillatory spike burst illustrates a gradual change in spike afterpotentials, with the most pronounced change at the somatic level (Fig. 4*A*). From one spike to the next, the fAHP and sAHP at the soma appear to decrease in amplitude, while the DAP grows in amplitude through the burst (Fig. 4*A*). The combination of DAP growth and AHP attenuation helps the cell reach threshold for a high frequency spike doublet. The spike doublet is then followed by a long burst afterhyperpolarization (bAHP) which terminates the burst (Fig. 4*A*).

MECHANISMS UNDERLYING AFTERPOTENTIALS

DAP Generation

The ability for backpropagating spikes to directly influence somatic membrane potential has become apparent in physiological and modeling studies (Zhang et al., 1993;

Turner et al., 1994; Mainen and Sejnowski, 1996; Wang, 1999). Turner et al. (1994) established that the generation of oscillatory spike bursts in pyramidal cells relies upon backpropagating Na^+ spikes that generate the DAP at the soma. A model depicting how a backpropagating spike influences somatic membrane excitability is shown in Figure 4*B*. Membrane depolarization initiates Na^+ spike discharge near the cell body and is followed by spike backpropagation through ~200 μm (approximately one-third) of the apical dendritic arborization. The somatic spike is of narrow duration while the dendritic spike rapidly increases in duration with distance from the soma. As a result, current associated with dendritic spike discharge sources back to evoke a DAP at the soma that is superimposed on the somatic fAHP and sAHP (Fig. 6*B*). It is important to emphasize that the DAP is generated primarily by electrotonic conduction *during* backpropagation of the spike from soma to dendrite, and not by a spike propagating in a return fashion from dendrite to soma.

AHP Generation

The conductances underlying AHPs in pyramidal cells are still unknown, although recent single channel and whole-cell recordings provide some indication as to the identity and distribution of the relevant ion channels. ELL pyramidal cells express the K^+ channels AptKv3.3 and AptKv3.1, homologues of Kv3.3 and Kv3.1 respectively (Rashid et al. 1999). Recent *in situ* hybridization studies show intense localization of AptKv3.3 channel in pyramidal cells (Rashid et al., 1999). Patch recordings in CMS pyramidal cells show an outward rectifying K^+ channel that has a high voltage for activation (~ -20 mV), ~25 pS conductance, high sensitivity to TEA and 4-AP (μM range), and very fast activation and deactivation (t~2 ms) (Morales et al., 1998). These characteristics are en-

tirely consistent with those of mammalian Kv3 channels (Kanemesa et al. 1995; Brew and Forsythe, 1995; Massengil et al. 1997). The kinetics of this channel and its localization to pyramidal cell somata make the AptKv3.3 current a likely candidate to both repolarize spike discharge and generate a fAHP at the soma.

The most likely candidate for sAHP and bAHP generation is a $K_{(Ca)}$ channel. In support of this, initial screening studies on CMS pyramidal cell somata and dendrites using single channel recordings have identified two Ca^{2+} activated K^+ currents, with single channel conductances of 180 pS and 90 pS (E. Morales, personal communication). Either or both of these channels may contribute to the sAHP or bAHP.

In summary, the ionic mechanisms underlying burst discharge in CMS pyramidal cells has not been fully determined. Burst discharge would appear to be driven by the rapid change in spike afterpotentials during repetitive discharge, while a spike doublet and bAHP terminates a burst, presumably to establish burst frequency.

HYPOTHESIS:

A progressive change in afterpotentials (fAHP, sAHP, DAP) during repetitive spike discharge underlies the burst depolarization, while generation of a spike doublet and bAHP controls the frequency of burst discharge.

OBJECTIVES:

The objectives of this study are as follows:

i) Characterize burst discharge in pyramidal cells to identify key elements which control burst frequency.

ii) Examine the mechanisms underlying somatic afterpotentials and burst termination.

Figure 3.

Representative examples of spike discharge generated by current injection at the soma (*A*) and in the apical dendrites (*B*). The soma exhibits both a fAHP and sAHP (*A*) while the dendrites exhibit only a small amplitude sAHP (*B*). *C*, Antidromic spikes recorded in separate somatic and dendritic recordings are shown superimposed, revealing a temporal correspondence between the dendritic spike and DAP. (*C*) shows the greater spike width in the dendrite as well as the greater spike amplitude and more pronounced fAHP and DAP in the soma. Abbreviations: fAHP, fast after hyperpolarization; sAHP, slow after hyperpolarization; DAP, depolarizing afterpotential.

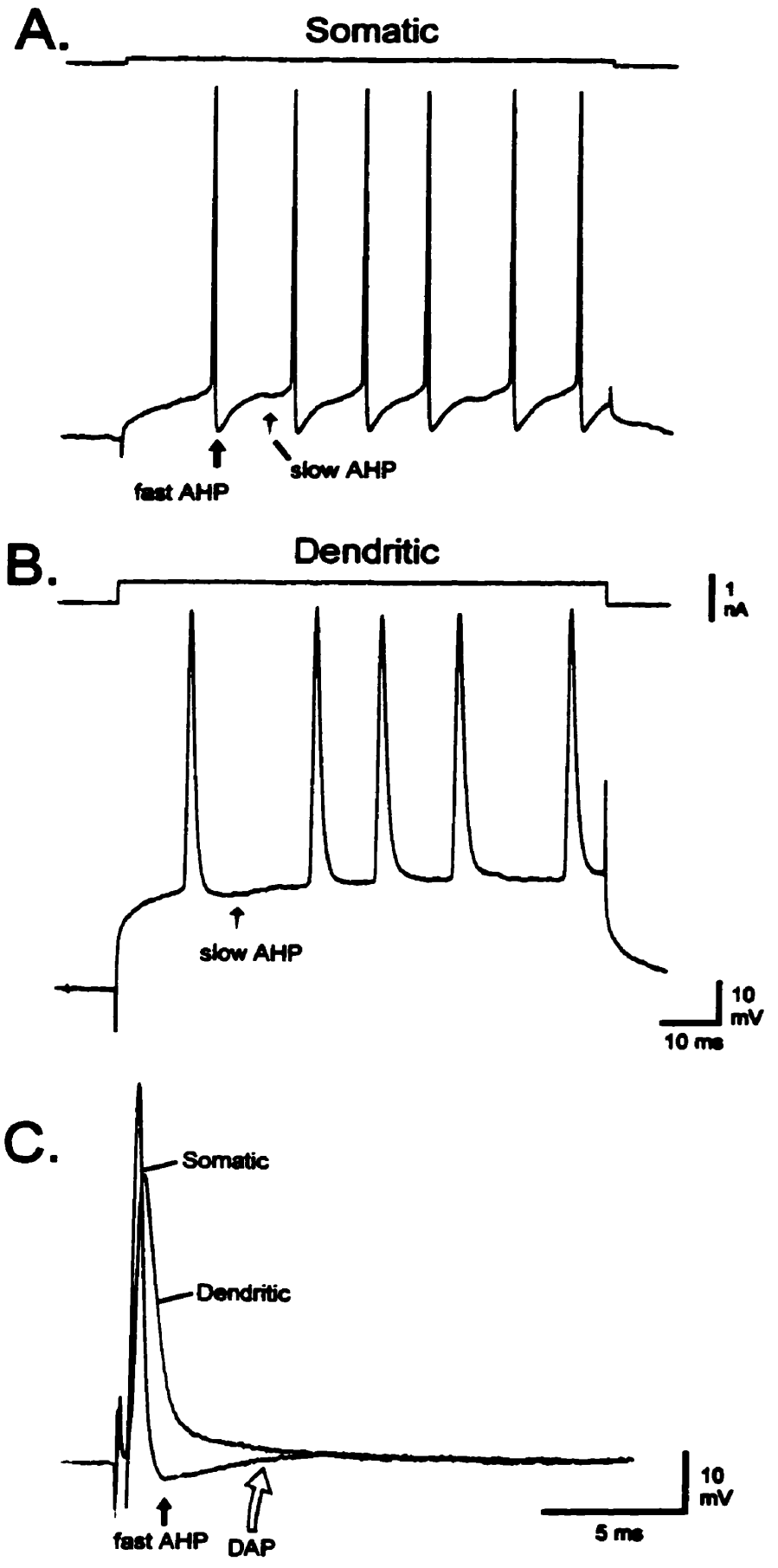
A.
Somatic
fast AHP
slow AHP
B.
Dendritic
1
nA
slow AHP
10
mV
10 ms
C.
Somatic
Dendritic
fast AHP
DAP
10
mV
5 ms

Figure 4.

A, A single current evoked spike burst at the soma indicating a progressive change in afterpotentials during repetitive spike discharge. The burst terminates when a spike doublet discharges (double linked arrows), which is followed by a subsequent large bAHP. *B*, Model of the mechanism for generating a DAP. Na^+ spike discharge is initiated at the soma (1), and backpropagates over the initial ~ 200 μM of the apical dendritic tree (2). Inward current underlying the long duration dendritic spike simultaneously sources back to the soma to generate a DAP following the somatic spike (3). Abbreviation: bAHP, burst after hyperpolarization.

A.

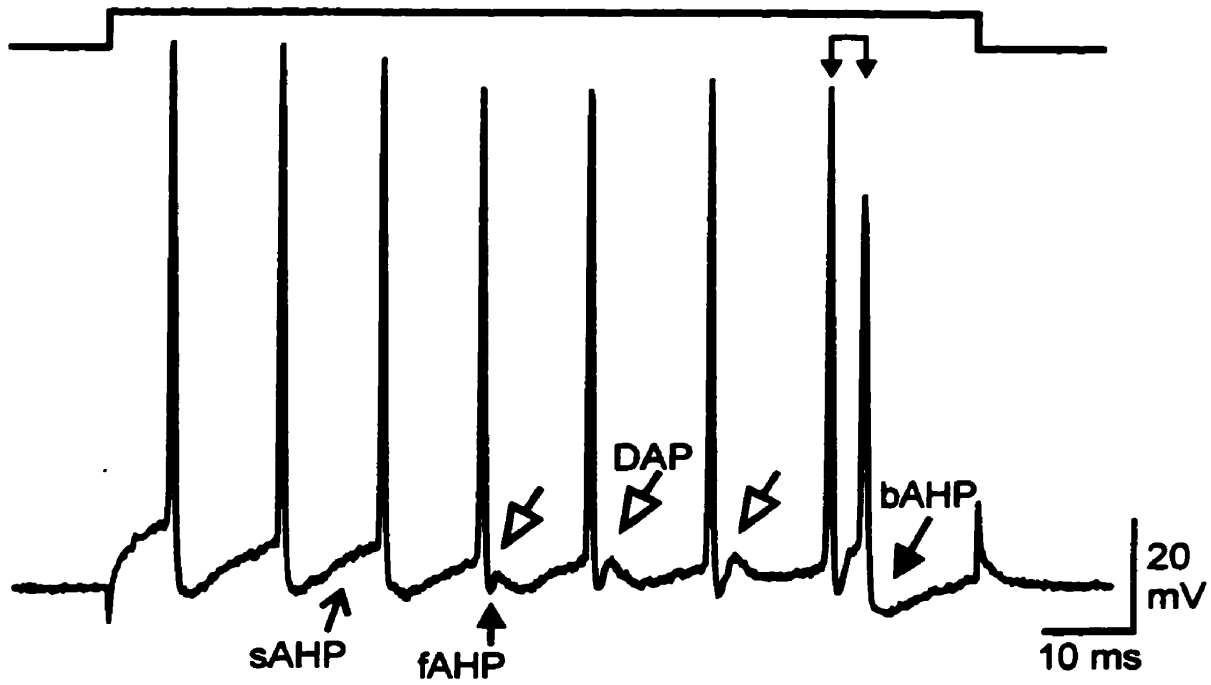

B.

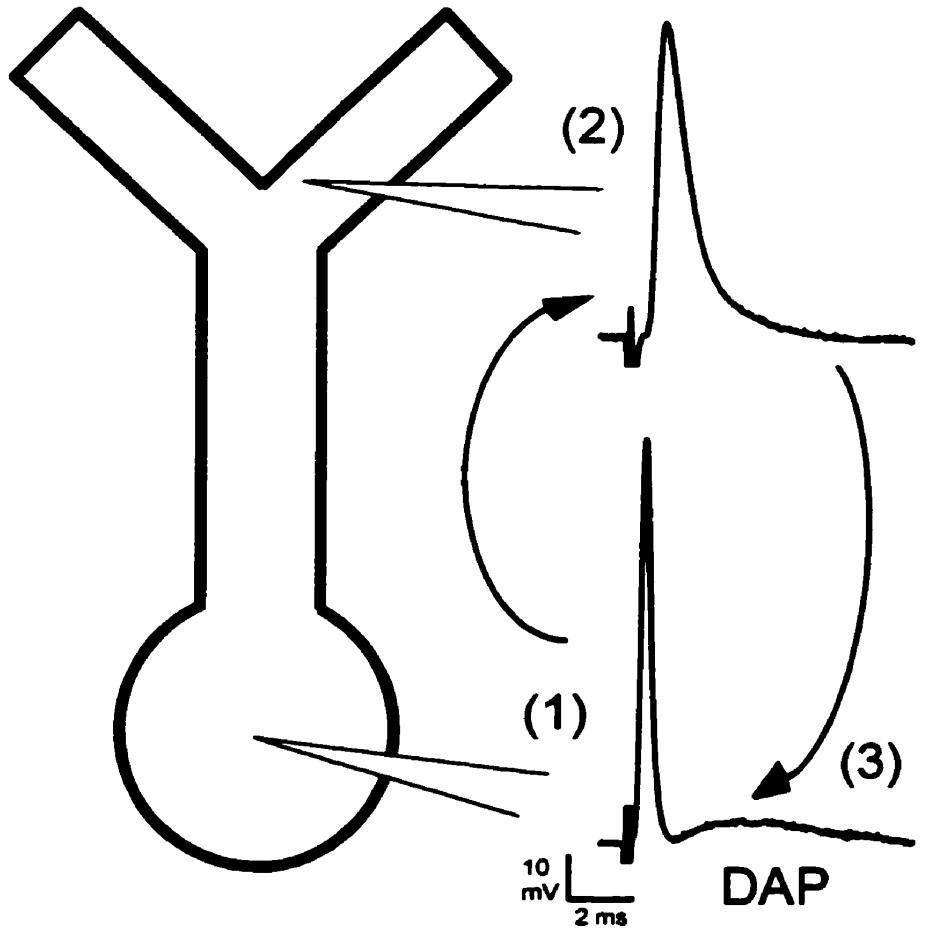

CHAPTER 2

METHODS AND MATERIALS

Preparation of *in vitro* Slices

Weakly electric gymnotiform fish *Apteronotus leptorhynchus* (Brown Ghost Knife fish) were obtained from local importers (Riverfront Aquariums) and maintained at 26-28 °C in aerated fresh water aquaria. All chemicals were obtained from Sigma (St. Louis, MO) unless otherwise noted. Recordings were obtained from pyramidal cell somata or apical dendrites using an *in vitro* slice preparation (Turner et al. 1994). Fish of 10-15 cm length were anaesthetized by immersion in aquarium water containing 0.05% 2,phenoxy-ethanol. The fish were then transferred to a custom-made stereotaxic apparatus for superfusion of gills with aerated aquarium water containing 0.05% 2,phenoxy-ethanol. The skin and cranium were removed with forceps and iridectomy scissors under microscopic observation (Olympus SZ-40) and the brain superfused with cold (4°C), oxygenated (95% O_2 / 5% CO_2), bicarbonate-buffered artificial cerebrospinal fluid (aCSF) consisting of (in mM): 124 NaCl, 2.0 KCl, 1.25 KH_2PO_4, 1.5 $CaCl_2$, 1.5 $MgSO_4$, 24 $NaHCO_3$, and 10 D-glucose, pH 7.4. A mini scalpel, consisting of a broken double-edged razor blade (J.B. EM Services Inc.) held within a blade breaker, was used to sever the anterior lateral line nerves and the spinal cord, and to transect the brain at the mid-tectal level at approximately 45° to the rostro-caudal axis. The caudal part of the brain was lifted out onto a spatula and the rostral surface of the brain attached with cyano-acrylate glue to a pre-cooled plastic block or the floor of a reduced metal Vibratome

chamber. To provide support to the brain during tissue slicing, the brain was surrounded with gelatin (20% in distilled water) ejected from a syringe previously warmed to ~40°C.

Tissue slices of 350-400 μm thickness were cut by Vibratome (Technical Products International) under microscopic observation along the transverse and then longitudinal axis into bicarbonate-buffered aCSF. In some cases, slices were cut in a reduced chamber filled with a sucrose-based aCSF consisting of (in mM): 218 sucrose, 25 $NaHCO_3$, 3.25 K Gluconate, 4.5 $MgCl_2$, 0.1 $CaCl_2$, 10 Glucose, and 1 Na Pyruvate (Kotecha et al., 1997). Excess gelatin was trimmed from slices using forceps and iridectomy scissors, and the slice floated onto a spatula for transfer to an *in vitro* slice chamber. Slices were perfused with bicarbonate-buffered aCSF as an interface preparation at room temperature and superfused with humidified 95% O_2 / 5% CO_2. Dissection was completed in ~15 min and tissue allowed 30-60 min for recovery and equilibration before recordings were carried out.

Stimulating and Recording Procedures

The majority of pyramidal cell recordings were obtained in the CMS topographic map. Since identification of these maps can be difficult in slices cut with a longitudinal orientation, a limited number of recordings may also have been obtained from the CLS or LS segments. Intracellular electrodes were pulled on a Campden Instruments 753 microelectrode puller from 1.5 mm outer diameter thick-walled borosilicate glass (A-M Systems Inc.). Microelectrodes were backfilled with 2 M $KC_2H_3O_2$ (pH 7.4; ~90 MΩ resistance) and the tips dipped in Aquasil (0.7% in distilled water)(Pierce Chemicals) two to three times over the course of an hour. Intracellular recordings were obtained from either pyramidal cell somata or apical dendrites using brief overcompensation of capacitance

neutralization. Unless otherwise indicated, all dendritic recordings were obtained ~150 μm from the cell body layer near the border between the tractus stratum fibrosum (tSF) and the molecular layer (Maler, 1979). All electrical activity was referenced to a Ag/AgCl bath ground. Voltage recordings were obtained in bridge mode (Axoclamp-2A; Axon Instruments) and were filtered over a bandwidth of DC - 10 kHz (2004-F, Intronix Technologies Inc.). Input resistance in somatic recordings was 73 ± 21.0 MΩ and in dendritic recordings between 74 ± 12.7 MΩ (n = 10 random samples)(Table 1). Direct current injection of -0.1 to -0.5 nA was applied when necessary to reduce spontaneous activity. Resting potentials at the soma were -77 ± 10 mV and in dendrites -76 ± 7.8 mV (n = 10 random samples) (Table 1).

Pyramidal cells were directly depolarized through the application of positive current steps through the recording electrode. Pyramidal cells were antidromically activated using square wave stimulus pulses (0.1 ms) delivered via an isolation unit (Digitimer SIU; 0.1 msec; 1 - 50 V) to a bipolar stimulating electrode consisting of twisted 62 μm nichrome wire placed in the plexiform layer. Antidromic stimulus trains were generated using a Master-8 programmable pulse generator (A.M.P.I.). Evoked activity was recorded and stored on a 486 PC for off-line analysis (Cambridge Electronic Design).

Focal Application of Channel Blockers

Extracellular recording electrodes were pulled on a Sutter Instruments P-87 micropipette puller from 1.5 mm outer diameter thin-walled borosilicate glass (A-M Systems Inc.). Electrode tips were broken back to 1-2 μm diameter against a platinum wire under microscopic observation. Channel blockers were added directly to a HEPES - buffered medium consisting of (in mM): 148 NaCl, 3.25 KCl, 1.5 $MgCl_2$, 10 Glucose, 10

HEPES, 1.5 $CaCl_2$. Drugs were then ejected to somatic and dendritic regions by applying air pressure pulses to the side port of the electrode holder (100-200 ms, 10-15 p.s.i., Medical Systems Inc.). A direct visual estimate of the diameter of the drug application was first obtained in molecular regions of cerebellum distant from the recording site, by adjusting the time and pressure for ejection to apply drugs over an approximate 50 μm initial diameter. Tetrodotoxin (TTX, 10 μM) (Alamone Labs), was focally ejected over restricted regions of the soma-dendritic axis. The tSF is a thick (100 μm) layer of mylinated fibers that overlies the pyramidal cell body layer (Maler, 1979) and acts as an effective barrier against drug diffusion between the pyramidal cell body and molecular layers. Evidence for this comes from delays of up to 2 min in detecting the effects of an ejected drug on potentials recorded from the other side of the tSF. In contrast, potentials recorded on the same side of the tSF can be affected within 2 sec.

Data Analysis

Statistical analysis was carried out using StatWorks (Cricket Software) and Microcal Origin (Microsoft) software. Average values are indicated as mean ± S.D. and statistical significance calculated using a student's T-test or the Wilcoxon Signed Ranks test. Data plots were fit by a sigmoidal or Gaussian function using the software Microcal Origin. The software Corel Draw (Corel Corporation) was used in figure preparation.

CHAPTER 3

RESULTS

SOMATIC AND DENDRITIC RECORDINGS

Somatic recordings were identified by action potential (AP) discharge of 50 - 80 mV of narrow duration and the presence of a fAHP and/or DAP. Dendritic recordings were distinguished by a typically smaller spike amplitude, longer spike duration and the lack of a distinct fAHP. The recording's location in the slice, its input resistance (Ri), resting membrane potential (RMP) and spike height were used to establish the cell's health. The Ri was calculated as the slope of a current/voltage (I/V) plot constructed for every recording obtained. The minimum health and quality of intracellular recordings were taken as a resting potential of at least -60 mV, input resistance over 46 MΩ and a spike height over 50 mV. Typical somatic and dendritic I/V plots and their respective current and voltage traces are represented in Figure 5. Somatic Ri ranged between 46–115 MΩ (73 ± 21.0 MΩ) and dendritic Ri ranged between 60–90 MΩ (74 ± 12.7 MΩ) (Table 1). Dendritic spike amplitude and width increased noticeably with recording distance although this was not strictly quantified. There were no corresponding changes in either RMP or Ri with recording distance from the soma. The recordings in this study are thus comparable to previous reports (Mathieson and Maler, 1988) (Turner et al, 1994, 1996) although Ri was significantly higher in the present study.

BURST CHARACTERISTICS

The occurrence of burst discharge in ELL pyramidal cells has been reported both *in vitro* and *in vivo* (Turner et al. 1994, 1996; Gabbiani et al. 1996; Metzner et al. 1998).

The present study extends this work by examining oscillatory spike bursts in both the soma and apical dendrites of pyramidal cells. Figure 6*A* illustrates that depolarizing current injection could evoke an oscillatory series of spike bursts in both somatic and dendritic recordings. Single spike bursts at the soma consisted of a series of spikes that steadily increased in frequency until generating a high frequency spike doublet of 200-350 Hz (Fig. 6*B*). The interspike interval (ISI) of spike doublets ranged from 2.5 – 10 ms and had a consistently shorter interval than the preceding spikes in the burst. The spike doublet was then followed by a large bAHP that separated individual spike bursts. Bursts were most often comprised of 5-7 spikes near threshold, but could consist of only spike doublets at the highest frequencies of burst discharge or at more depolarized membrane potentials. The basic pattern and frequency of oscillatory spike bursts were similar at the somatic and dendritic level, a result consistent with a site for spike initiation at the soma (Turner et al., 1994). The dendritic sAHP and bAHP were smaller in amplitude than at the soma. In many cases the dendritic sAHP could not be detected, while the bAHP could consist of only a pause in spike discharge during a slow decay of membrane potential over 10 – 20 ms following the spike doublet (Fig. 6*B*) (Table 1). Oscillatory discharge in either pyramidal cell somata or apical dendrites is thus defined as a repeating series of spike bursts with subsequent bAHPs, where individual spike bursts are terminated by a high frequency spike doublet.

During a spike burst there was a net increase in membrane depolarization in soma and dendrites that further drove spike generation (Fig. 6*B*). This shift in the balance between depolarizing and hyperpolarizing spike afterpotentials was most visible for somatic recordings, where the fAHP and sAHP decreased in amplitude while the DAP increased

in amplitude with each successive spike. This produced a net shift in membrane potential of up to 5.3 mV during burst discharge at the soma (2.8 ± 1.4 mV; $n = 9$). Repetitive discharge converted the small dendritic sAHP to a net depolarization of up to 9.8 mV (6.2 ± 2.84 mV; $n = 9$; Fig. 6*B*). Following the bAHP, the amplitude of the fAHP and sAHP partially recovered by the first spike of the next burst, allowing the process to begin again (Figs. 6, 8*B*).

FACTORS CONTRIBUTING TO BURST GENERATION AND FREQUENCY

Pyramidal cells exhibit a differential frequency selectivity to sensory input *in vivo* that differs between the ELL topogaphic maps (Shumway, 1989). There is evidence that several characteristics of burst discharge change across these maps *in vitro* in a manner consistent with this frequency selectivity (Turner et al., 1996). I focused on identifying factors which determined burst threshold, and the range of oscillatory frequencies exhibited by cells in the CMS topographic map.

Burst Generation

The tendency for pyramidal cells to exhibit oscillatory spike bursts was assessed by constructing frequency/current (F/I) curves ($n = 70$). Since the pattern and frequency of discharge was entirely equivalent in somatic and dendritic recordings, these numbers have been pooled in the following analyses. Pyramidal cells responded to depolarizations near spike threshold with a relatively tonic discharge of Na^+ spikes in the pattern of an initial lag and subsequent increase in frequency (Fig. 7*A*) (Mathieson and Maler, 1988; Turner et al., 1994). As depolarizing current was increased (80 ms; 0.1 - 1.2 nA), 61% of recordings shifted from tonic to burst discharge, revealing an intensity-dependent shift in the pattern of spike output ($n = 43 / 70$). Although some cells exhibited burst discharge

upon initial spike generation, there was typically a clear threshold for burst discharge at a higher level of the F/I curve (Fig 7*B*). This most often corresponded to ~70% of the maximum spike frequency attained on the F/I curve. The frequency of spike bursts at the threshold for bursting was consistently between 10-60 Hz (34 ± 10.8 Hz; n = 28). As current injection was increased burst frequency increased and the population exhibited two clear frequency distributions at the maximal current level that could be fit by two Gaussian peaks of 49.8 ± 14.9 and 95.8 ± 28.1 Hz (Fig. 7*C*). The reason for two distributions at high levels of current injection is unknown, but could relate to the maximal level of current injected, or evidence for a difference in burst properties between basilar and non-basilar pyramidal cells. The range of oscillatory burst frequencies recorded for individual cells over the full extent of an F/I curve varied widely between 10-140 Hz (51 ± 40.2 Hz; n = 28) (Fig. 7*D*). By comparison, spike frequency (not including the spike doublet) ranged between 25-60 Hz at threshold for spike discharge and increased up to 475 Hz at higher levels of current injection.

An interval histogram of the average ISI at burst threshold revealed a clear relationship between spike ISI and the switch from tonic to burst discharge (Fig. 7*E*). Bursts were evoked most readily when the ISI fell within 3-7 ms (125 - 300 Hz; mean of 5.5 ± 1.38 ms, n = 34). There was also an inverse relationship between the absolute current level at burst threshold and cell Ri (r = -.59; n = 34; data not shown). However, Ri was not highly correlated with the qualitative characteristics of burst output, including the oscillatory frequency at burst threshold (r = .23) or the oscillatory burst frequency range (r = . 25; n = 25).

Table 1.

The average value of membrane properties, and the amplitude and duration of evoked spikes and afterpotentials in pyramidal cell somata and apical dendrites (≥ 150 μm). Average values are mean ± S.D. and n = 10 samples taken at random from the available cases. All measurements of spike parameters and afterpotentials were taken in reference to the membrane potential immediately preceding discharge of the spike when evoked near threshold intensity. DAP measurements were taken from antidromic spikes evoked at resting potential. Statistical comparisons were made between corresponding values obtained in somatic and dendritic recording sites.

	RMP	Ri	Spike	fAHP	sAHP	DAP	bAHP
Soma	-77 ± 10 mV	73 ± 21 MΩ	65 ± 10 mV 1.2 ± 0.36 ms	5.6 ± 2.7 mV 1.2 ± 0.5 ms	2.5 ± 1.2 mV 6.7 ± 3.9 ms	3.2 ± 1.5 mV 10.7 ± 2.0 ms	9.1 ± 1.5 mV 10.4 ± 4.2 ms
Dendrites	-76.7 ± 7.8 mV	74 ± 12.7 MΩ	51.7 ± 10.6 mV 3.9 ± 0.89 ms	N/A	0.92 ± 0.49 mV 10.6 ± 4.3 ms	N/A	2.8 ± 2.1 mV 8.5 ± 4.5 ms

Figure 5.

Left column shows both current (I) and voltage (V) traces for a somatic (*A*) and dendritic *(B)* intracellular recording. From the current and voltage traces current – voltage (I/V) plots are constructed and the Ri calculated as the slope of the linear portion of the data. Right column shows the corresponding I/V plots at the soma (Ri = 85 MΩ) and dendrite (Ri = 77 MΩ).

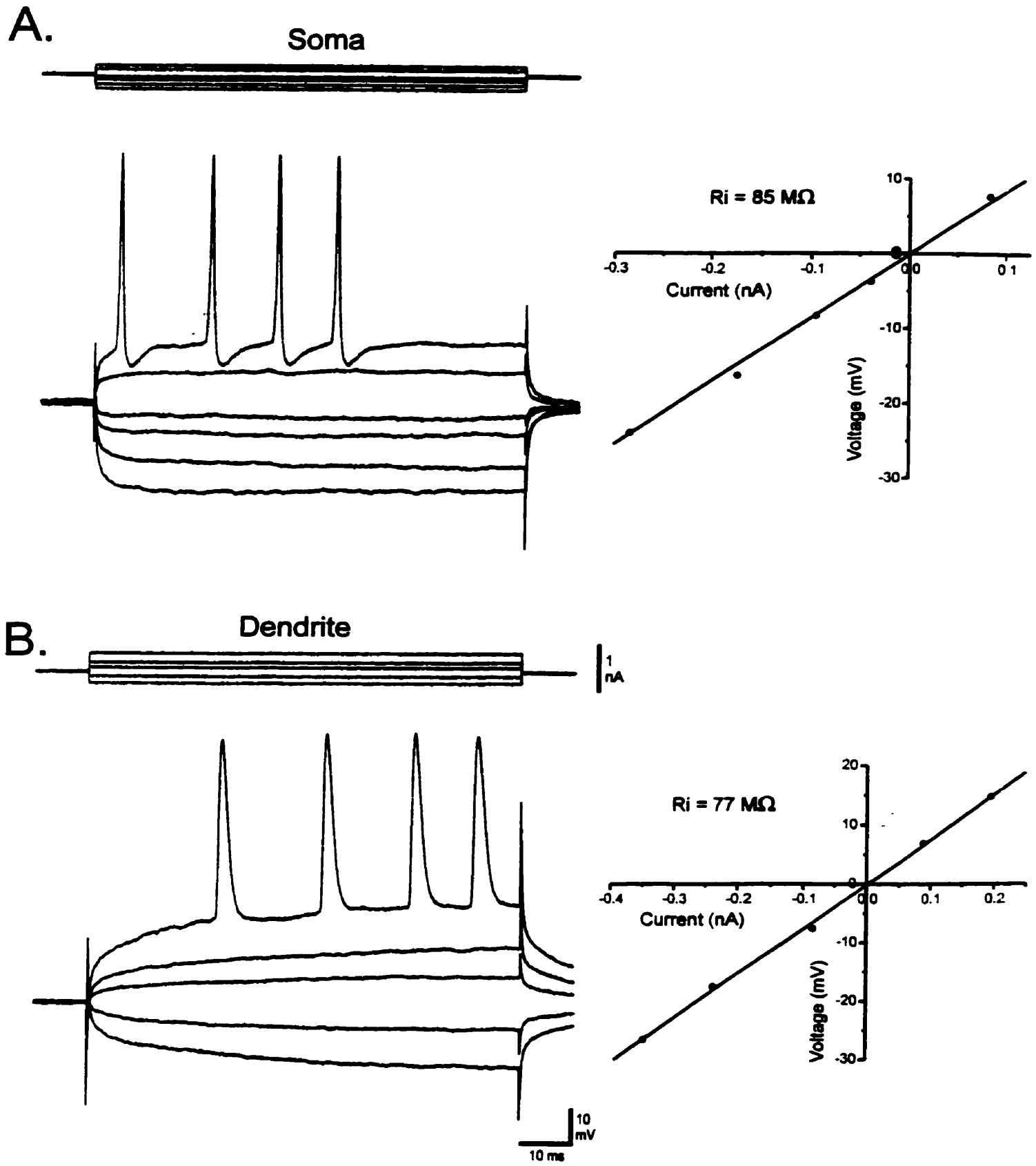
A.
Soma
Ri = 85 MΩ
10
-0.3
-0.2
-0.1
0.0
0.1
Current (nA)
-10
-20
-30
Voltage (mV)
B.
Dendrite
1
nA
Ri = 77 MΩ
20
10
0
-0.4
-0.3
-0.2
-0.1
0.0
0.1
0.2
Current (nA)
-10
-20
-30
Voltage (mV)
10
mV
10 ms

Figure 6.

A, Representative examples of oscillatory spike bursts evoked by direct current injection in a separate pyramidal cell somatic and apical dendritic recording. Oscillatory discharge in each location is comprised of a series of spike bursts separated by bAHPs (*arrows*). *B*, Expanded views of representative single spike bursts in separate dendritic and somatic recordings (somatic spikes truncated, and bursts are approximately aligned to facilitate comparisons). At the soma there is a pronounced reduction in AHPs (*solid arrows*) and an increase in DAP amplitude (*open arrows*) during a spike burst. A comparatively small sAHP in dendrites is reduced as dendritic spikes summate to produce an underlying membrane depolarization during a burst. Bursts are terminated upon the generation of a high frequency spike doublet (*double linked arrows*) and large amplitude bAHP at the soma. The doublet pair in dendrites consists of a full dendritic spike and a pre-potential, followed by the bAHP. One oscillatory period is defined as the combined duration of the spike burst and subsequent bAHP (*dashed lines below recording traces*).

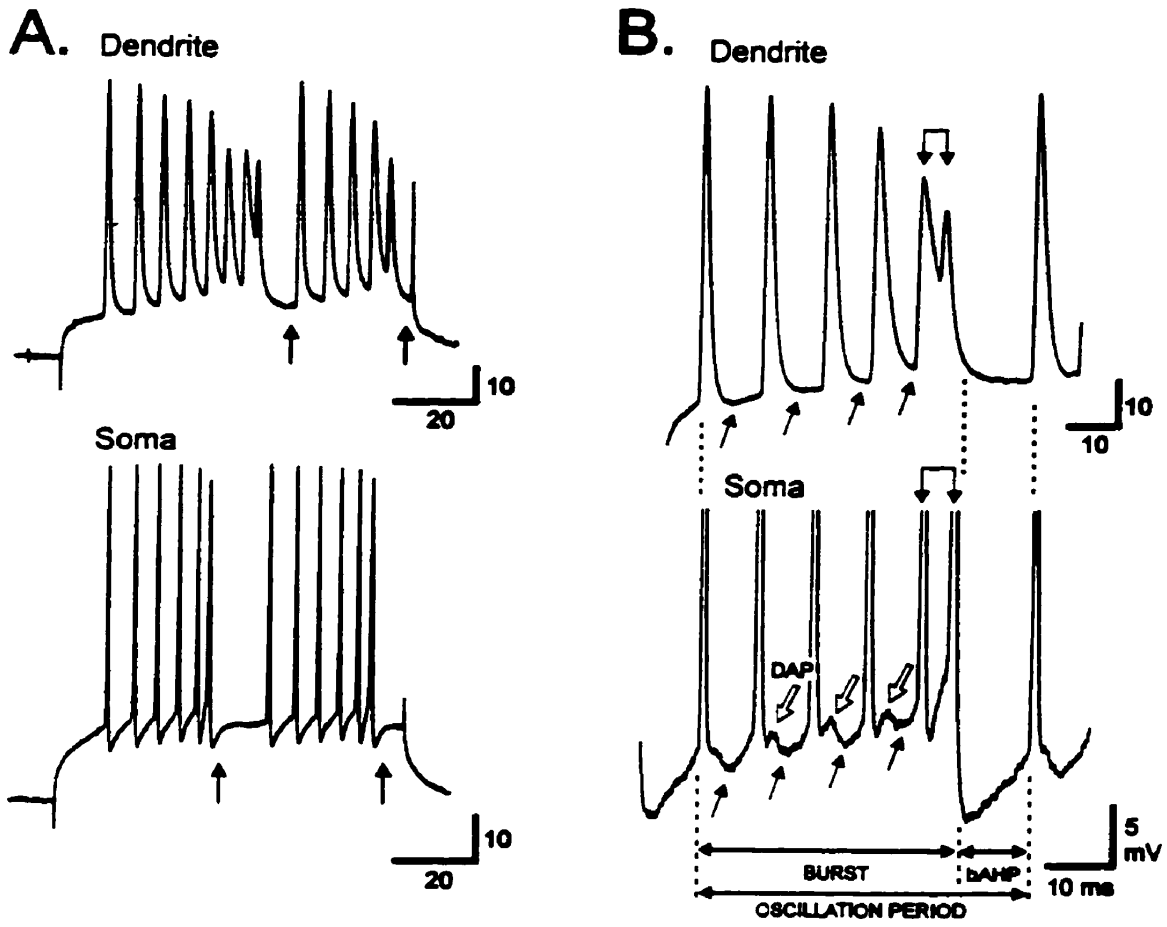
A.
Dendrite
10
20
Soma
10
20
B.
Dendrite
10
10
Soma
DAP
5
mV
10 ms
BURST
sAHP
OSCILLATION PERIOD

Figure 7.

Pyramidal cells exhibit an intensity-dependent shift in spike output from a tonic to burst discharge. *A*, A shift from tonic to burst output in a pyramidal cell somatic recording as the level of depolarizing current injection was increased (bAHPs separating spike bursts are denoted by arrows). Numbers indicate corresponding positions on the frequency/current (F/I) curve shown in *B*. *B*, F/I curve of spike discharge for the recording shown in *A* with the threshold for transition to oscillatory spike bursts marked by an arrow (80 ms current pulse). The F/I curve could typically be fit as a sigmoidal function. *C*, Interval histograms of oscillatory burst frequencies recorded at burst threshold (white bars) and at the maximum of the F/I curve (shaded bars). The data were fit by Gaussian function to a peak value of 34 ± 9.8 Hz at burst threshold and at high intensity with two Gaussian fits of 49.8 ± 14.9 and 95.8 ± 28.1 Hz (n = 28; Binwidth = 10). *D*, Interval histogram of the range of oscillatory burst frequencies exhibited by individual cells over the full F/I curve. *E*, Interval histogram of the average interspike interval recorded at burst threshold, indicating a link between interspike interval and the shift from tonic to burst output. Burst threshold was most often reached when interspike intervals fell between 3 - 8 ms. Data were fit by a Gaussian function to a peak value of 5.5 ± 1.38 ms (n = 32 soma; n = 11 dendrites; Binwidth = 1).

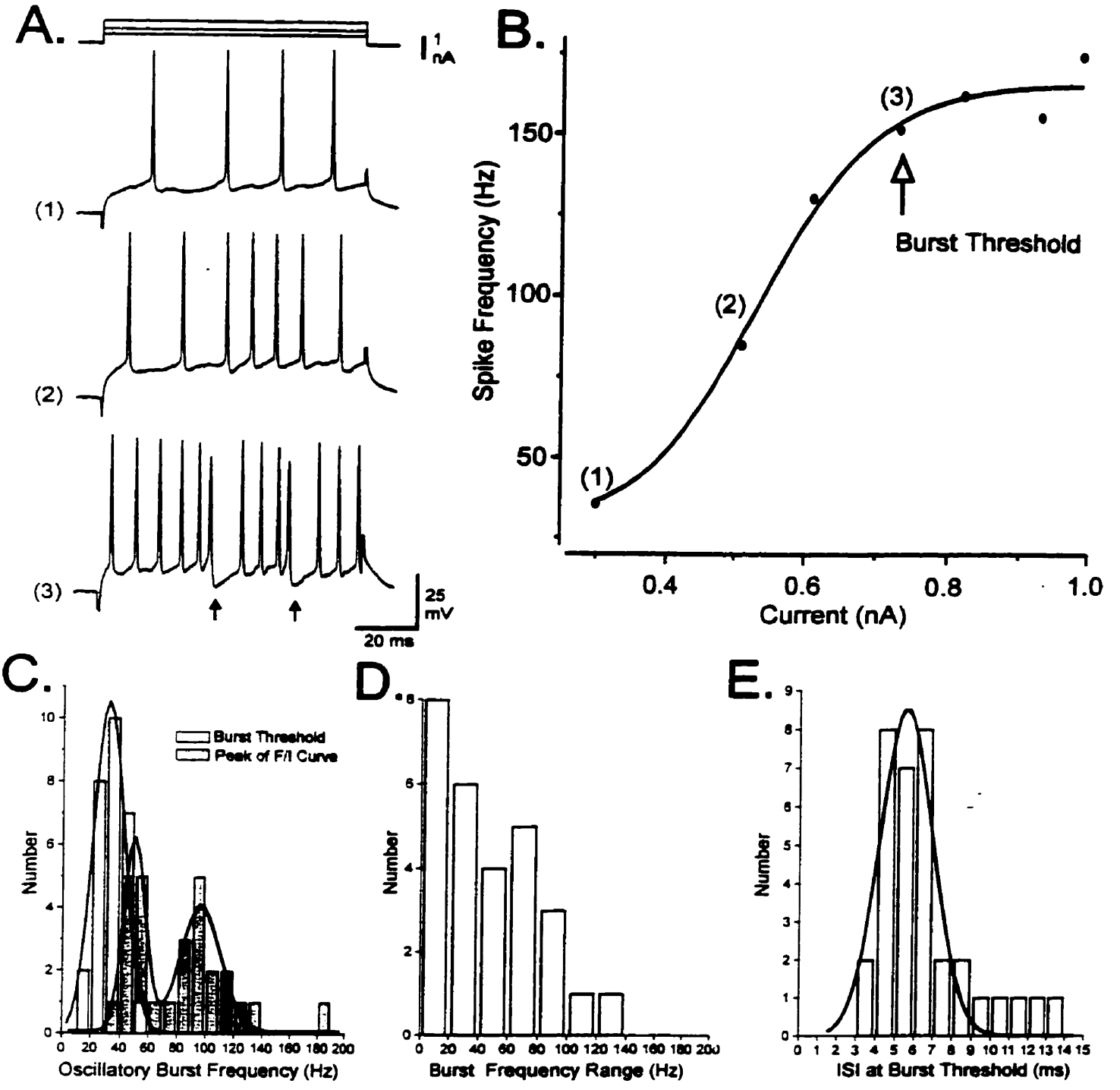
A.
1 nA
(1)
(2)
(3)
25 mV
20 ms
B.
Spike Frequency (Hz)
150
100
50
(1)
(2)
(3)
Burst Threshold
0.4
0.6
0.8
1.0
Current (nA)
C.
Burst Threshold
Peak of F/I Curve
Number
Oscillatory Burst Frequency (Hz)
D.
Number
Burst Frequency Range (Hz)
E.
Number
ISI at Burst Threshold (ms)

Pyramidal cells could also shift from tonic to burst output during current-evoked depolarizations, indicating a time-dependent change in the pattern of spike output (n = 30) (Fig. 8*A*). Once initiated, the frequency of oscillatory spike bursts increased over time to reach an eventual steady state. Figure 8*B* illustrates such a frequency shift in a somatic recording during a 4 s current pulse initially set subthreshold for burst discharge. In this cell, oscillatory bursts of ~20 Hz began 750 ms after current pulse onset, and increased to ~50 Hz by the end of a 4 s current pulse (Fig. 8*C*). As found during the construction of F/I curves, the shift in tonic to burst output was associated with a decrease in ISI during repetitive discharge. This corresponded to ISIs of 8.8-12.5 ms (9.9 ± 0.64 ms; n = 4) during the initial stage of tonic spike discharge, and a shift to burst output as the ISI stabilized to ~8.7 ms or below (8.7 ± 0.14 ms; n = 4).

These studies indicate that burst discharge has a clear threshold which can be attained in a voltage- or time-dependent manner that depends on spike discharge reaching an ISI of ~3-7 ms. The shift from tonic to burst discharge in pyramidal cells was thus strongly dependent on spike frequency.

Burst Frequency

I next examined the parameters of burst discharge in CMS pyramidal cells that are regulated to effect the wide range of oscillatory burst frequencies (10-140 Hz) shown in Figures 7 and 8. A shift in oscillatory burst frequency could involve a change in the properties of spike discharge during the burst itself, a change in the subsequent bAHP, or in both elements. The ability to evoke a progressive increase in oscillatory burst frequency in pyramidal cells with long depolarizations allowed me to identify these pa-

rameters. These studies revealed a pronounced but selective change in several aspects of the spike burst but not the bAHP in pyramidal cells.

During long membrane depolarizations, the number of spikes per burst decreased as oscillatory burst frequency increased, eventually leading to a series of bursts comprised of only 2-3 spikes 1-2 s after current pulse onset (Fig. 8*D*). The duration of spike bursts also decreased as oscillatory frequency increased, stabilizing to a relatively fixed duration once the bursts had been reduced to 2-3 spikes (Fig. 8*E*). This pattern of change in burst parameters was detected in all cells examined in relation to either the duration or amplitude of membrane depolarizations. However, a sequential analysis of burst discharge uncovered the surprising result that the duration of the bAHP showed little or no change as oscillatory burst frequency increased (Fig. 8*E*).

Figures 9-12 present an in-depth analysis of burst discharge for the cell shown in Figure 8 to establish which parameters in the spike burst or bAHP were most clearly correlated to the shift in oscillation period over time.

Spike burst

I first considered factors within the spike burst (Fig. 9*A*), including:

- burst duration
- the number of spikes per burst (excluding spike doublets)
- the mean ISI during a burst
- the net depolarization within the burst (burst amplitude)
- the net change in membrane depolarization during a burst over time – (defined as burst slope).

Figure 8.

Pyramidal cells exhibit a time-dependent shift in spike output from tonic to burst discharge. *A,B,* Somatic recording of a cell shifting to burst discharge during a current pulse initially set subthreshold for bursts. Arrows denote bAHPs as the cell began to burst (A, 750 ms) and at progressively longer time points after the onset of a 0.74 nA, 4 s current pulse (*B*; numbers correspond to times shown in *C*). *C,* A plot of oscillatory burst frequency vs time illustrating an increase from ~20 Hz to ~50 Hz during the current pulse. *D,E,* The increase in oscillatory frequency was associated with a decrease in the number of spikes per burst (*D*) and a decrease in burst duration (*E*). There was little or no change in the duration of the bAHP as oscillation frequency increased (*E*). Single somatic recording, $n = 100$ spike bursts. Variations in spike height in A and B are due to a low sampling rate.

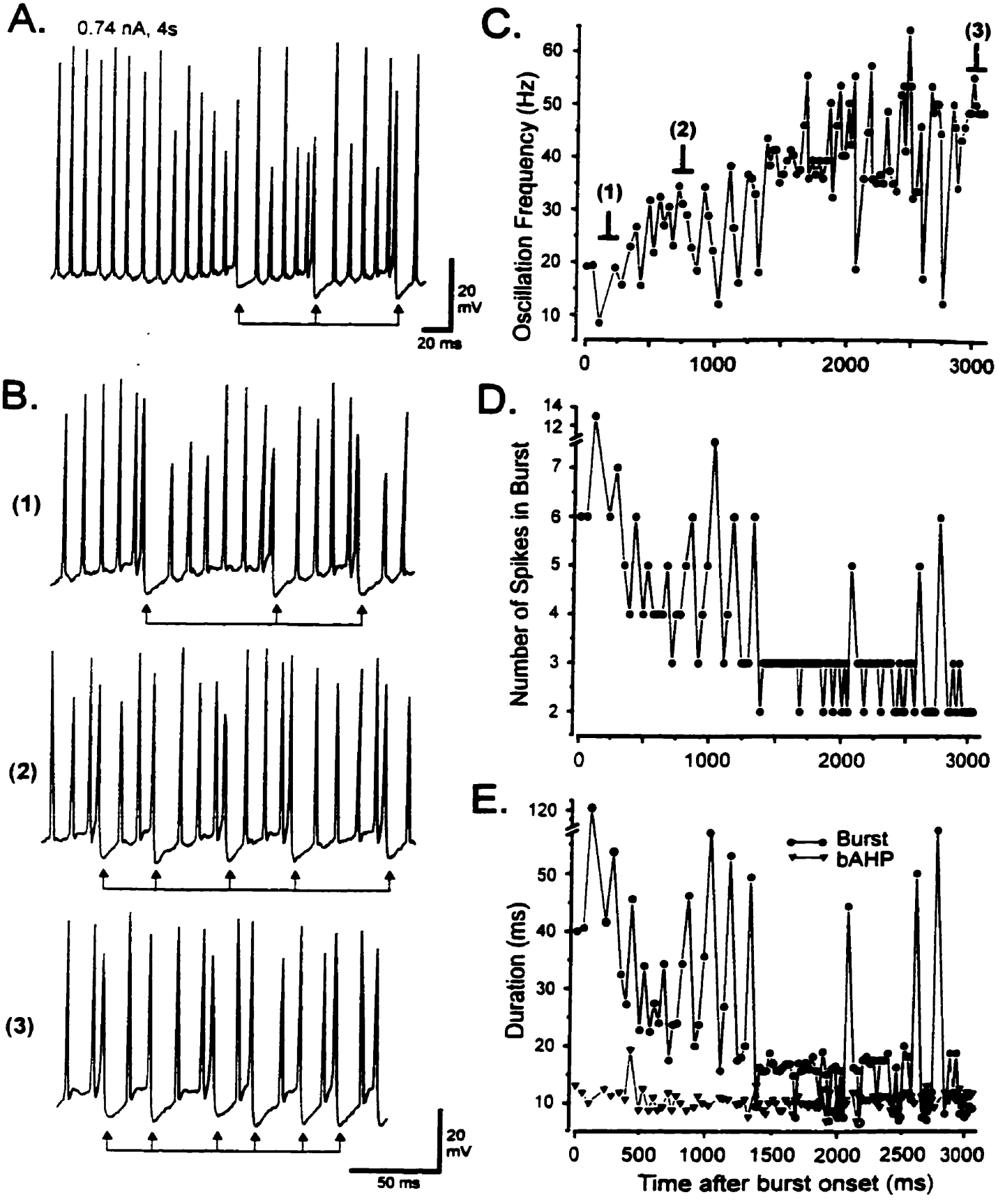
A.
0.74 nA, 4s
20 mV
20 ms
B.
(1)
(2)
(3)
20 mV
50 ms
C.
Oscillation Frequency (Hz)
(1)
(2)
(3)
D.
Number of Spikes in Burst
E.
Burst
bAHP
Duration (ms)
Time after burst onset (ms)

Figure 9.

Specific intraburst parameters are correlated to changes in oscillation period. Data is taken from the cell shown in Figure 8. *A*, A single spike burst indicating areas of measurement (m, burst slope; A, burst amplitude). Spikes are truncated for illustrative purposes. *B-D*, Oscillation period was highly correlated to burst duration (*B*), the number of spikes per burst (*C*), and burst slope (*D*; expressed in Figures 10-12 as 1/burst slope, ms/mV). Single somatic recording, $n = 100$ spike bursts. The correlation coefficients (r) are shown on each graph.

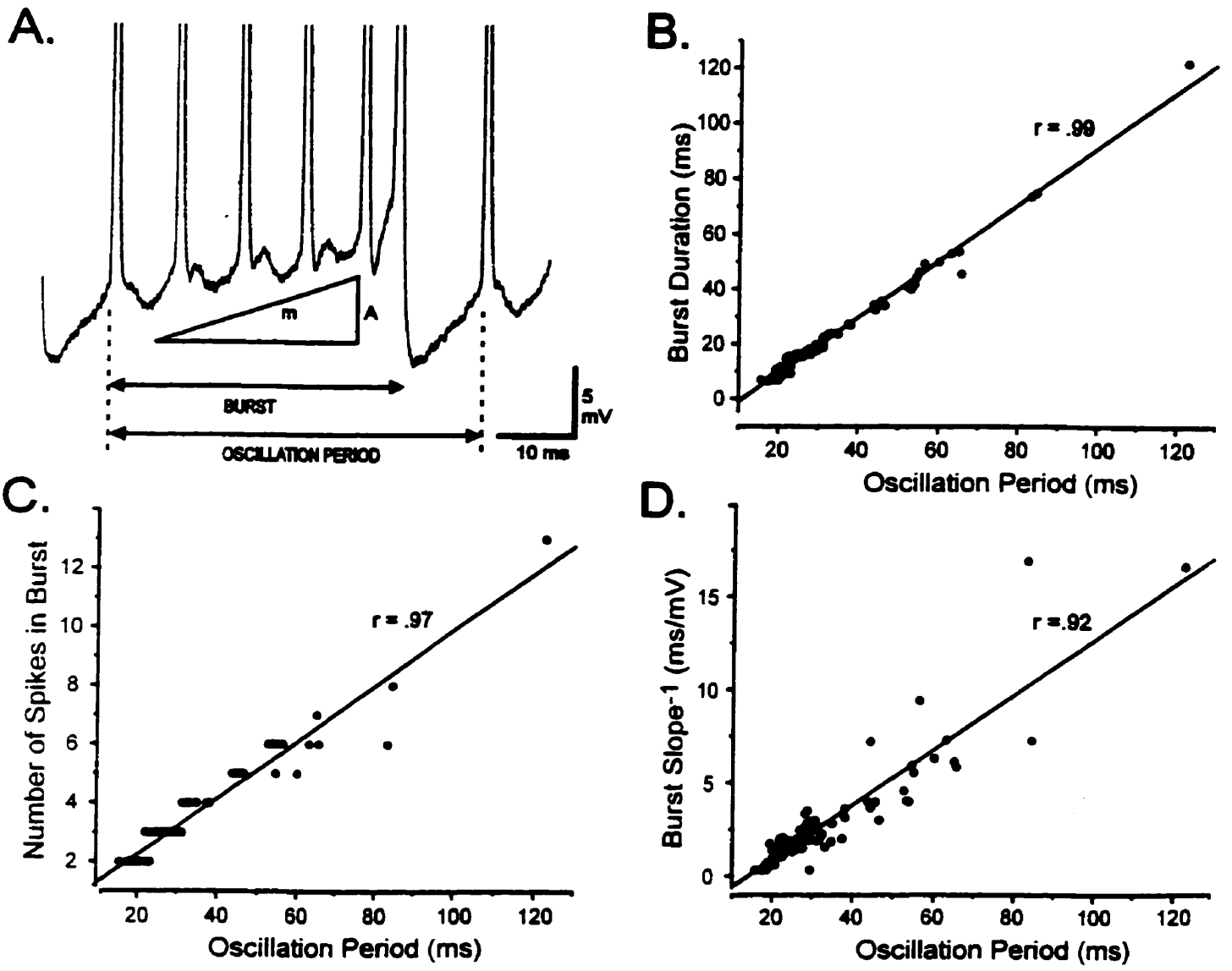
A.
m
A
BURST
OSCILLATION PERIOD
5
mV
10 ms
B.
Burst Duration (ms)
Oscillation Period (ms)
r = .99
C.
Number of Spikes in Burst
Oscillation Period (ms)
r = .97
D.
Burst Slope-1 (ms/mV)
Oscillation Period (ms)
r = .92

Figure 10.

Intraburst parameters that were not correlated to oscillation period. *A,B*, No significant correlation was found between oscillation period and burst amplitude (*A*) or the mean ISI (*B*). *C,D*, The voltage threshold for generating a spike doublet shows no consistent change with an increase in oscillatory frequency over time (*C*), and was not correlated to a change in oscillation period (*D*).). Single somatic recording, $n = 100$ spike bursts. The correlation coefficients (r) are shown on each graph.

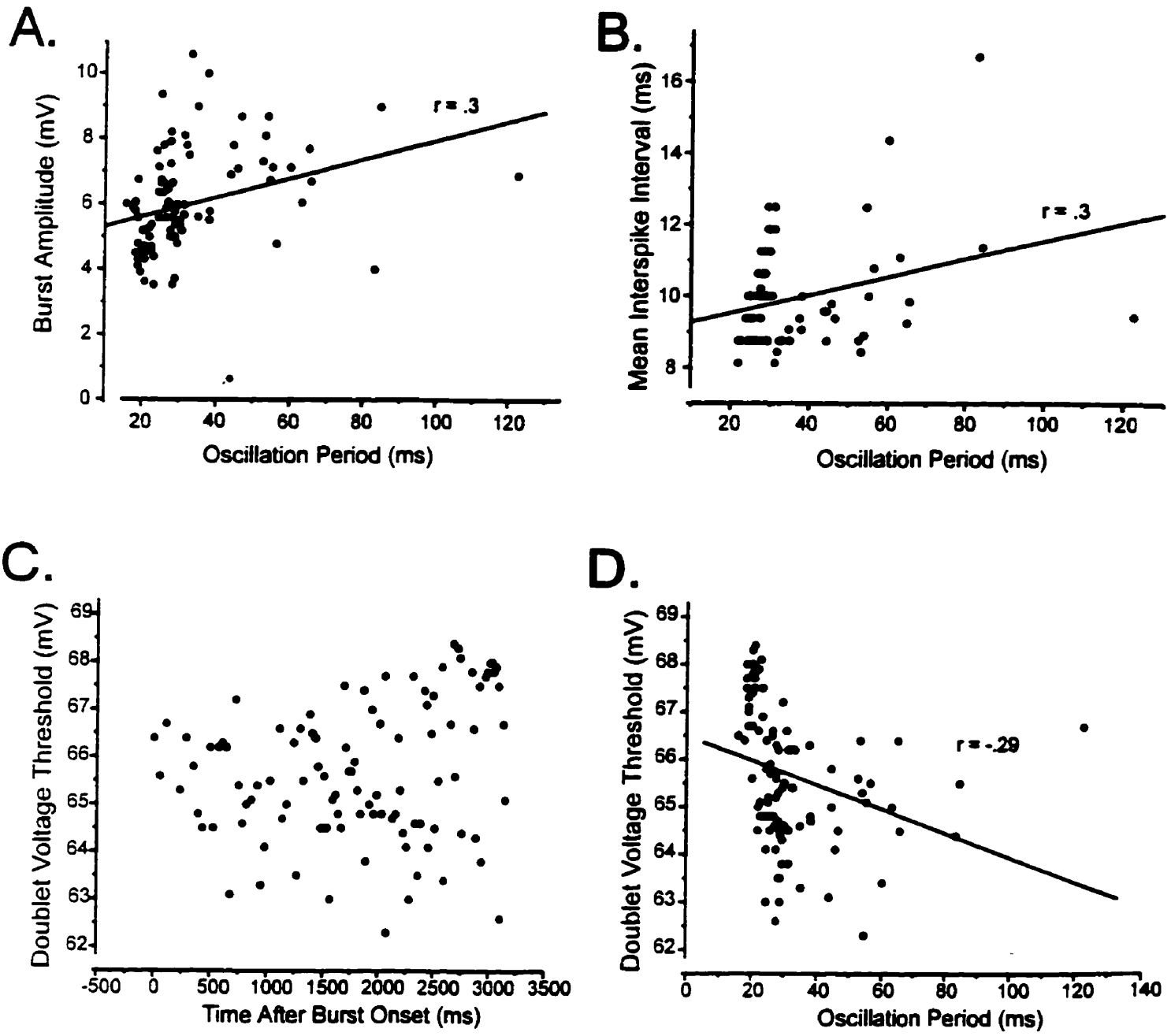
A.
Burst Amplitude (mV)
r = .3
Oscillation Period (ms)
B.
Mean Interspike Interval (ms)
r = .3
Oscillation Period (ms)
C.
Doublet Voltage Threshold (mV)
Time After Burst Onset (ms)
D.
Doublet Voltage Threshold (mV)
r = -.29
Oscillation Period (ms)

Figure 11.

Specific intraburst parameters are correlated to changes in burst duration. Data is taken from the cell shown in Figure 8, with measurement parameters as shown in Figure 9*A*. *A,B,* Burst duration was highly correlated to the number of spikes per burst (*A*) and burst slope (*B*). *C,D,* No significant correlation was found between burst duration and either burst amplitude (*C*) or mean ISI during the burst (*D*). The mean ISI was calculated from bursts comprised of 4 or more spikes and do not include the spike doublet). Single somatic recording, n = 100 spike bursts. The correlation coefficients (r) are shown on each graph.

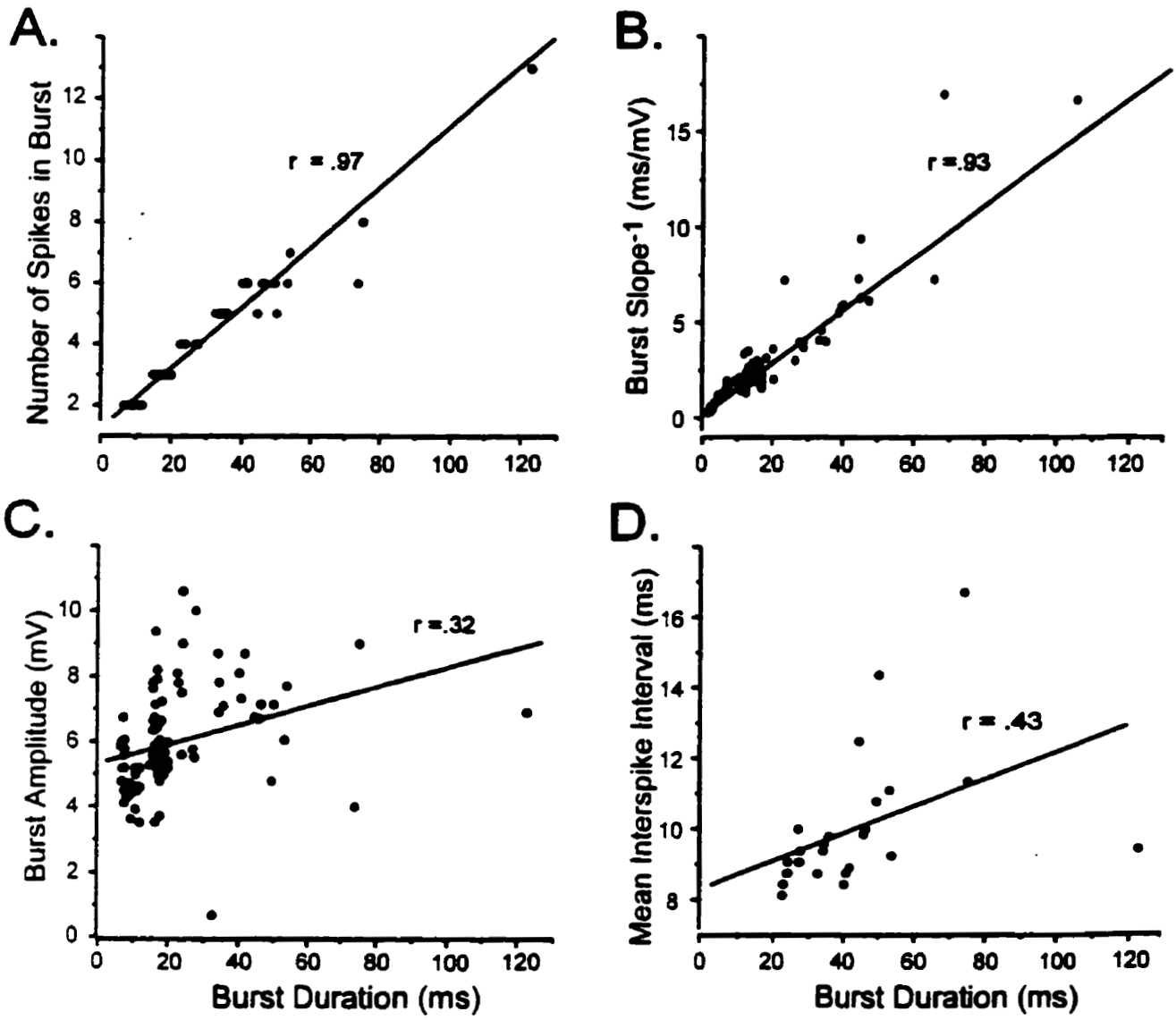
A.
Number of Spikes in Burst
r = .97
B.
Burst Slope-1 (ms/mV)
r = .93
C.
Burst Amplitude (mV)
r = .32
Burst Duration (ms)
D.
Mean Interspike Interval (ms)
r = .43
Burst Duration (ms)

Figure 12.

The bAHP is not correlated to oscillation period, or to factors within the burst. Data is from the cell shown in Figure 8. A single spike burst indicating areas of measurement (*A*). The oscillation period was not significantly correlated to the bAHP amplitude (*B*), or bAHP duration (*C*). The bAHP duration was not correlated to burst duration (*D*), the number of spikes in a burst (*E*), or the burst slope (*F*). Single somatic recording, $n = 100$ spike bursts. Abbreviations: m, slope; A, amplitude.

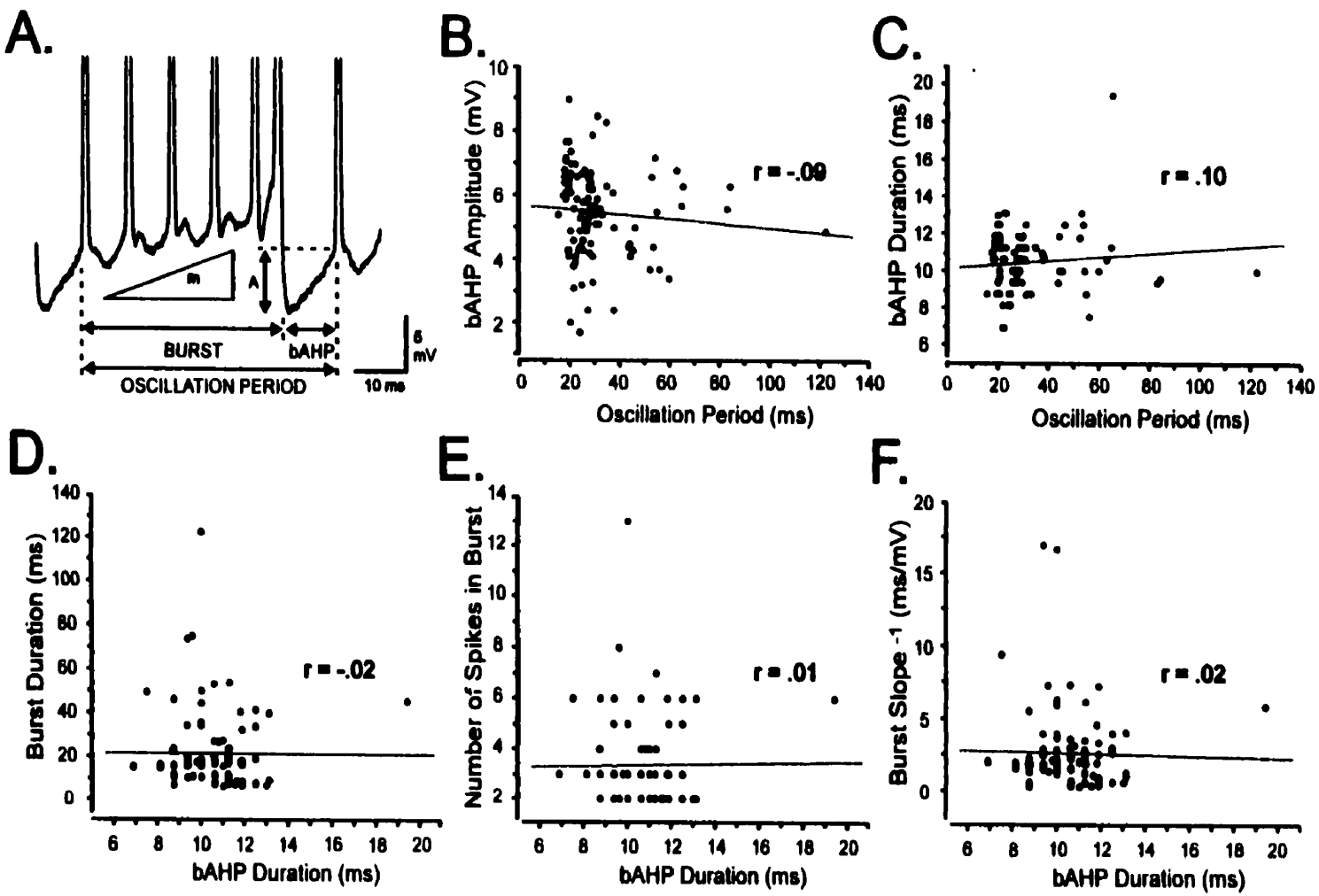
A.
m
A
BURST
bAHP
OSCILLATION PERIOD
5 mV
10 ms
B.
bAHP Amplitude (mV)
r = -.09
Oscillation Period (ms)
C.
bAHP Duration (ms)
r = .10
Oscillation Period (ms)
D.
Burst Duration (ms)
r = -.02
bAHP Duration (ms)
E.
Number of Spikes in Burst
r = .01
bAHP Duration (ms)
F.
Burst Slope -1 (ms/mV)
r = .02
bAHP Duration (ms)

Three factors were very highly correlated to oscillation period: (i) burst duration, (ii) the number of spikes per burst, and (iii) burst slope (Fig. 9*B-D*). In contrast, oscillation period was not correlated to either burst amplitude (Fig. 10*A*) or the mean ISI (Fig. 10*B*) within each burst. The absolute voltage threshold for the spike doublet showed no consistent change over time (Fig. 10*C*), and was not correlated to oscillation period (Fig. 10*D*).

A closer examination of the burst itself revealed that burst duration was also highly correlated to the number of spikes per burst and burst slope (Fig. 11*A,B*) but not to burst amplitude or the mean ISI within each burst (Fig. 11C,*D*).

bAHP

The consistency of the bAHP observed during a shift in oscillatory burst frequency (Fig. 8*E*) was verified by the finding that oscillation period was not correlated to either bAHP amplitude or duration (Fig. 12*B,C*)(Lemon et al., 1998). In addition, none of the factors examined within the preceding burst appeared to influence the characteristics of the bAHP, including burst duration, the number of spikes in the burst, or the burst slope (Fig. 12*D-F*); all of which were highly correlated with changes in oscillation period (Fig. 9). Moreover, bAHP characteristics were not correlated to the properties of spike discharge in the subsequent burst, as might be predicted in cells controlling burst discharge through an interplay between the currents I_h and I_T (McCormick and Huguenard, 1992; Huguenard, 1996; Pape, 1996). Thus, the bAHP appeared to be generated almost independently of oscillation period.

The bAHP is only generated after a spike doublet. I therefore looked more closely at the relationship between the spike doublet and bAHP to try and identify some factor

which could control bAHP generation. Figure 13 demonstrates that bAHP amplitude did have a detectable relationship with the specific ISI of the spike doublet (Fig. 13*A*). The bAHP amplitude appeared to be greatest over a narrow range of spike doublet ISIs (5-7 ms), with the degree of variability increasing outside of this range. A similar but weaker relationship was observed for bAHP duration over the same range of spike doublet ISIs (Fig. 13*B*). Although these trends are not as compelling as those relating intraburst properties to oscillation period, the spike doublet ISI remains the only factor that I have identified to date which can be related to the characteristics of the bAHP. Regardless, this may be significant, as the short ISI of the spike doublet could be an important factor controlling Ca^{2+} influx and any Ca^{2+} - activated K^+ conductance which might underlie the bAHP.

Model of mechanisms controlling oscillatory burst frequency

The data presented in Figures 8-11 allow the formulation of a model of how pyramidal cells produce a shift in oscillation period (Fig. 14). Since one oscillation period is defined as the combined duration of a spike burst and bAHP (Fig. 14*A*), a change in oscillation period could arise through changes in the properties of one or both of these elements. Since the bAHP appeared to be generated almost independently of oscillation period, factors within the burst are sufficient to account for a shift in oscillation period.

Burst duration was one of the factors most highly correlated to oscillation period. One of the most important factors controlling burst duration is the generation of a spike doublet, which terminates the burst with a bAHP. Burst duration is thus highly dependent on the cell reaching threshold for the spike doublet. Neither the threshold for generating a spike doublet nor the burst amplitude exhibited any change in relation to oscilla-

tion period. Therefore the *time* required to attain threshold for the spike doublet becomes the important variable. This time can be varied by changing the rate (slope) of membrane depolarization within a burst. If burst slope is increased, the threshold for generating a spike doublet is attained in a shorter period of time, thereby reducing burst duration (Fig. 14*B*). A change in burst duration also accounts for the number of evoked spikes per burst, as a progressively shorter burst duration will sequentially reduce the number of spikes discharged. Therefore, the *slope of the depolarization* within the burst can be identified as the critical determinant of burst duration, the number of spikes per burst, and oscillation period. This in turn relates to the degree of interaction between the somatic DAP and afterhyperpolarizations during repetitive spike discharge.

CHANGES IN AFTERPOTENTIALS DURING REPETITIVE DISCHARGE

Given the clear change in spike afterpotentials during burst discharge (Fig. 6*B*), I examined more closely the underlying basis for the change in fAHP, sAHP, and DAP amplitudes during repetitive discharge.

AHPs

As superimposition of the DAP and AHPs prevented quantification in intact cells, a method to "isolate" somatic AHPs from the DAP was required. It was previously shown that the somatic DAP can be reduced by focally ejecting TTX in the mid-dendritic region (Turner et al., 1994). However, these earlier experiments did not attempt to block the discharge of all dendritic Na^+ spikes, including those in the most proximal dendrites. I thus modified this procedure to block all spike backpropagation to examine somatic AHPs in the absence of a DAP. To ensure that all dendritic activity was blocked, TTX ejections were continued until TTX had diffused to the cell layer and affected the somatic

spike. By restricting my measurements to those records obtained immediately prior to this time, I was able to examine somatic AHPs in relative isolation.

Repeated ejections of TTX (10 - 15 μM) in the dendritic region blocked the DAP and prevented the shift in membrane potential necessary to generate a spike doublet and bAHP, effectively blocking oscillatory spike bursts (Fig. 15). This established that both the somatic fAHP and sAHP were very stable in amplitude and duration throughout a spike train, even though spike frequency remained similar to that in control recordings (Fig. 15*B*; $n = 5$). These data are important in revealing that somatic AHPs do not contribute to the change in afterpotentials observed during repetitive discharge; either through a cumulative inactivation of underlying currents, or by a shift in E_K. We were unable to perform a similar test on the dendritic sAHP, but the small amplitude or lack of this response in dendrites suggests that it has a minor influence compared to that of somatic AHPs. The experiments illustrated in Figure 15 thus indicate that most if not all of the change in somatic afterpotentials during burst discharge can be attributed to changes in the DAP.

DAP

Based on the model of DAP generation in Figure 4*B*, one can predict that an increase in the degree of dendritic depolarization during a burst could enhance DAP amplitude at the soma. I therefore compared somatic and dendritic spikes during burst discharge. This revealed a small but statistically insignificant decrease in somatic spike amplitude (92 ± 7.9% of control; $n = 9$) and no change in the rate of somatic spike repolarization or duration over the time course of a single burst (Fig. 16*A,C*).

Figure 13.

bAHP properties are correlated only to the ISI of the spike doublet. Data is taken from the cell shown in Figure 8 during a long duration current pulse. The bAHP amplitude (*A*) is greatest over only a narrow range of spike doublet ISIs (5-7 ms). The bAHP duration (*B*) appears to have a more consistent length over a specific range of doublet ISI's (5-8 ms). $n = 100$ spike bursts.

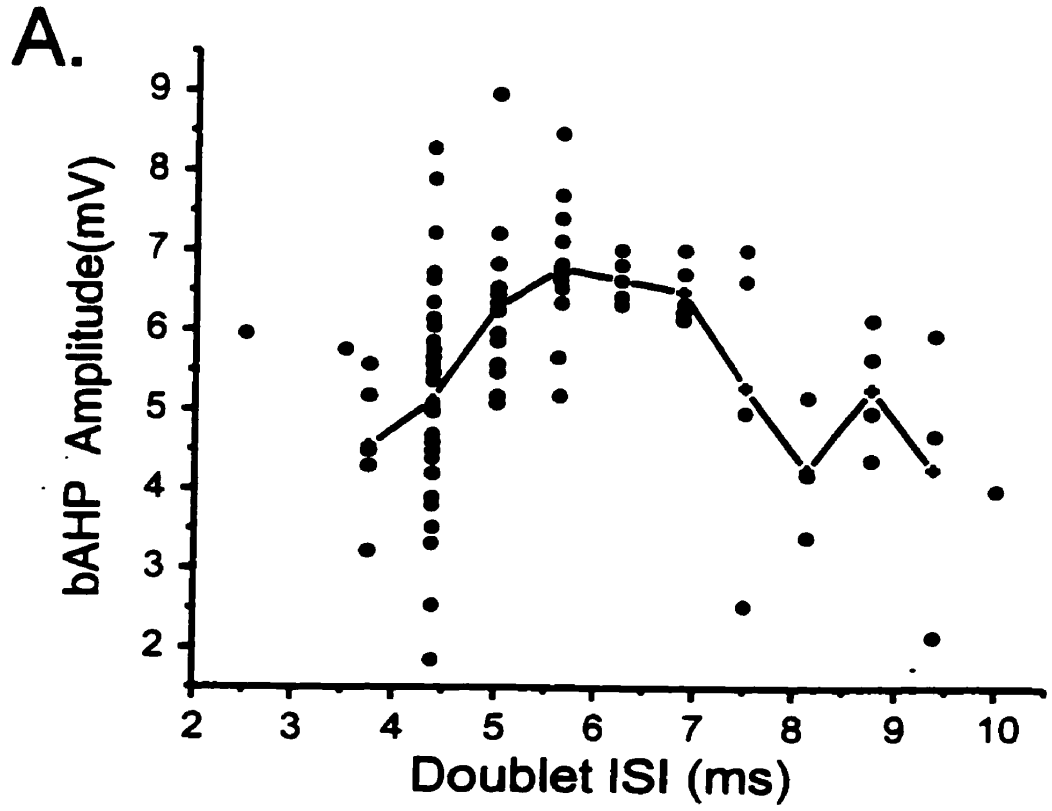
A.
bAHP Amplitude(mV)
9
8
7
6
5
4
3
2
2
3
4
5
6
7
8
9
10
Doublet ISI (ms)

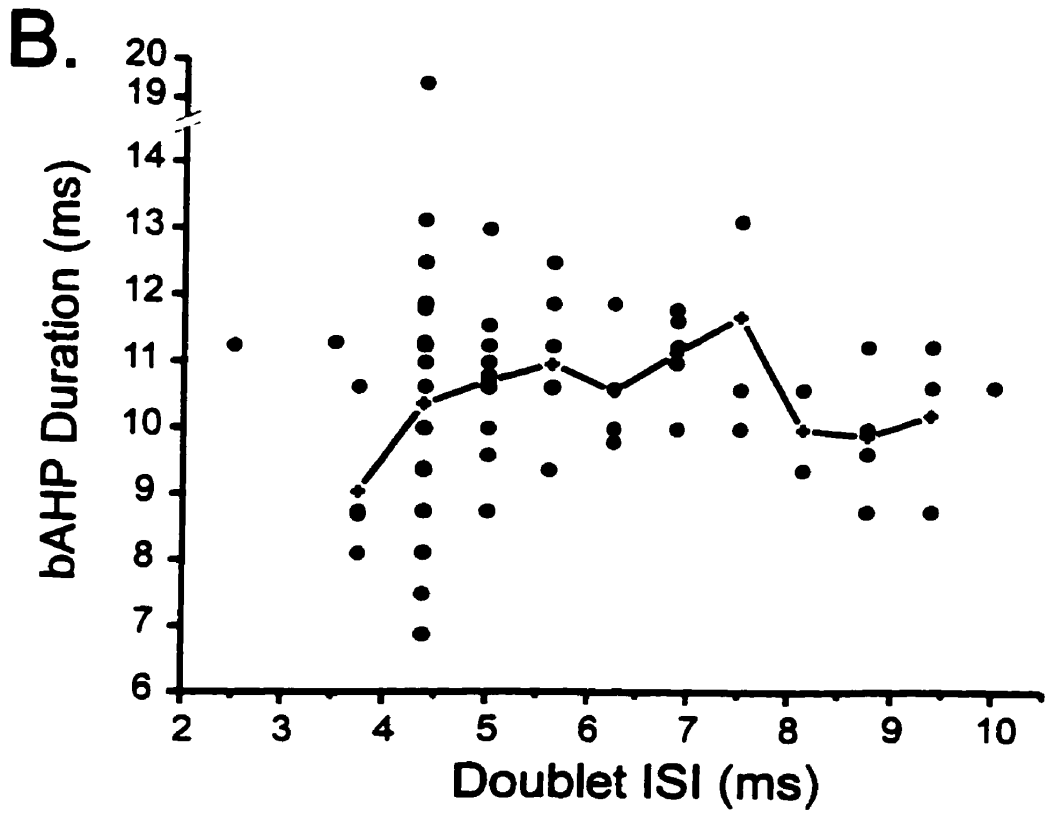
B.
bAHP Duration (ms)
20
19
14
13
12
11
10
9
8
7
6
2
3
4
5
6
7
8
9
10
Doublet ISI (ms)

Figure 14.

Model of the parameters controlling oscillation period in pyramidal cells. *A,B,* Representative traces of single spike bursts in a somatic recording exhibiting an oscillation period of 54 ms in *A* and 43 ms in *B*. Spikes are truncated for illustrative purposes. A burst slope of 0.11 mV/ms in *A* increases to a rate of 0.16 mV/ms in *B* (large arrow), allowing the depolarization within the burst to reach threshold for a spike doublet in a shorter period of time. As a result, the onset of the bAHP shortens burst duration from 36 ms to 25 ms, reduces the number of spikes per burst from 6 to 4, and reduces oscillation period. There is no identifiable change in bAHP characteristics as oscillation period is reduced. Therefore, the primary factor controlling oscillation period is the burst slope, reflecting the degree of interaction between the DAP and AHPs that lead to the generation of a spike doublet.

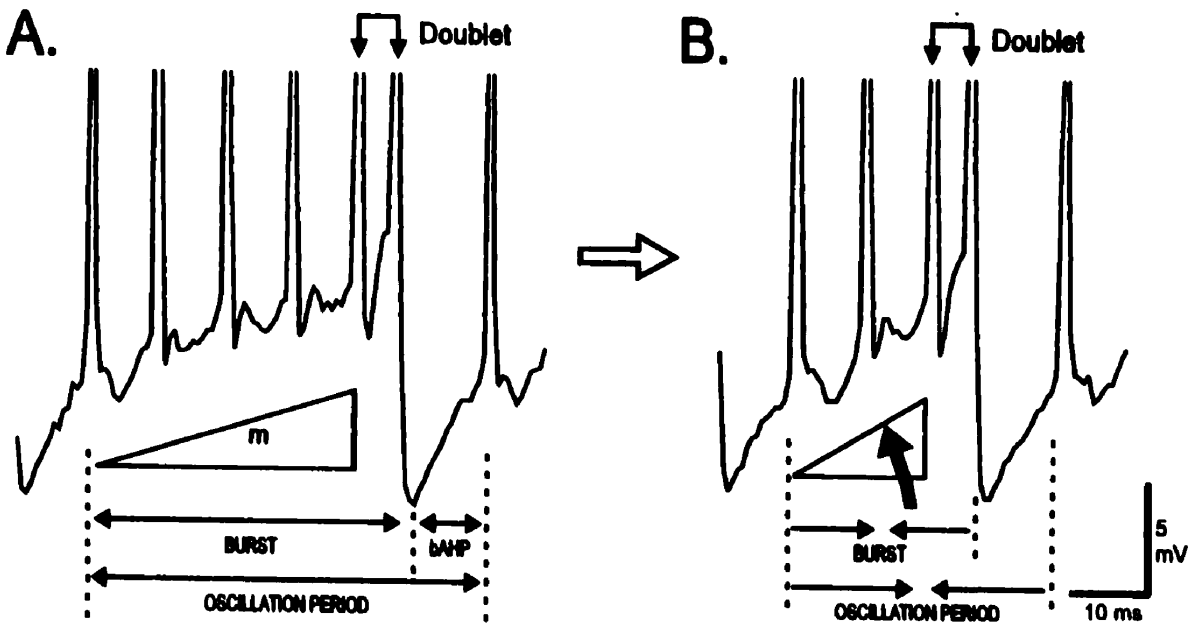

Burst Slope = .11 mV/ms
Number of spikes = 6
Burst Duration = 36 ms
Oscillation Period = 54 ms

Burst Slope = .16 mV/ms
Number of spikes = 4
Burst Duration = 25 ms
Oscillation Period = 43 ms

In contrast, dendritic spikes exhibited a greater decrease in amplitude during a burst (65 ± 11.7% of control; $n = 9$; $p < .001$, Student's T-test), and a substantial change in both the rate of repolarization and duration (Fig. 16*B*). By the third spike of a burst, the rate of repolarization of dendritic spikes could decrease to 66% of control values while spike duration increased up to 135% (measured at 10% above baseline) (Fig. 16*C,D*).

Since repetitive spike discharge in pyramidal cells exhibits a gradual increase in frequency during a burst, I examined the possibility that the increase in dendritic spike width during a burst was frequency-dependent. These experiments employed antidromic stimulus pairs delivered at varying condition-test (C-T) intervals to determine any frequency-dependent change in the DAP or dendritic spike. As shown in Figure 17, there was a pronounced effect on both the DAP and dendritic spike over a specific range of C-T intervals. At the soma, antidromic C-T intervals of ~2.2 - 2.9 ms fell within the spike refractory period and blocked spike discharge. C-T intervals of 2.9 - 3.2 ms reduced DAP amplitude on the test response (Fig. 17*A*; $n = 8$), an effect which could be seen as an all-or-none phenomenon in some cases. In contrast, C-T intervals of ~3 - 7 ms markedly potentiated the DAP by up to 500% (Fig. 17*A,C*). As the potentiated DAP was often large enough to reach spike threshold, a spike doublet was effectively evoked at these C-T intervals (Fig. 17*A*). Potentiation of the DAP was most apparent in terms of absolute amplitude but could also be detected as an increase in duration. Measurements of peak DAP amplitude revealed an average maximal increase of 262 ± 121% between 2.6 - 5.5 ms C-T intervals, which then decreased to 120 ± 13% ($n = 8$) at a 10 ms C-T interval. The potentiation of DAP amplitude gradually decreased at longer C-T intervals, but was still present in one case as a 134% increase at a 60 ms C-T interval. It is important to

note that neither the reduction nor the potentiation of DAP amplitude can be attributed to recurrent activation of synaptic responses, as pyramidal cell axons exhibit no recurrent collateral projections (Maler, 1979; Maler et al., 1981).

In dendritic recordings antidromic C-T intervals of 3.0 - 4.5 ms evoked the test response upon the falling phase of the control dendritic spike, and near the dendritic spike refractory period. As a result, the amplitude of the test dendritic spike was gradually reduced as C-T intervals were shortened to ~3.0 ms. At the shorter of these C-T intervals a small pre-potential of 26.6 ± 9.5 mV and 2.4 ± 0.4 ms (n = 8) was uncovered (Fig. 17*B*). Earlier work has established that a similar pre-potential recorded in dendrites represented the passive reflection of a spike discharged at the soma (Turner et al., 1994). In agreement with this, C-T intervals of ~2.1 - 2.9 ms blocked the small pre-potential in dendrites in an all-or-none manner, as found for the somatic spike (data not shown). As C-T intervals fell beyond ~4.5 ms, dendritic spike amplitude began to approach control values, but exhibited a substantial decrease in the rate of repolarization and an increase in duration. This produced a temporal summation of the spike pair, and often resulted in the discharge of a spike doublet on the test response, as indicated by the presence of a pre-potential (Fig. 17*B*, lower trace). The onset latency of this pre-potential (~3-4 ms) coincided with an increase of 158 ± 46.3% in the absolute voltage shift on the test dendritic spike (n = 8; $p < .01$; Wilcoxon Signed Ranks test) (Fig. 17*D*). This increase in dendritic potential gradually declined with longer C-T intervals, but could still be detected in some recordings at C-T intervals as long as 20 ms (Fig. 17*D*). Importantly, there was a close correspondence between the peak amplitude of the somatic DAP and the dendritic spike voltage over a wide range of C-T intervals (Fig. 17*C*,*D*).

The changes I observed in DAP amplitude and dendritic spike waveforms for paired stimuli continued to accumulate during repetitive spike discharge. As shown in Figure 18*A*, DAP amplitude and the temporal summation of dendritic spikes steadily increased during an antidromic stimulus train. This led to the eventual generation of a spike doublet, as evidenced by a full amplitude spike pair at the soma and a spike followed by a small pre-potential in dendrites. I found that three to four antidromic stimuli delivered at 150 - 200 Hz could evoke increases of up to 350% in peak DAP amplitude and 250% in the absolute dendritic potential at the estimated peak of the somatic DAP (Fig. 18*B*). Furthermore, summation of dendritic spikes during repetitive stimulation affected the threshold for burst discharge, as indicated by the generation of a spike doublet. Thus, increasing the number of spikes in an antidromic stimulus train enabled a longer ISI (lower spike frequency) to evoke a spike doublet (Fig. 18*C,D*).

It is important to note that the C-T intervals tested in the above experiments are of direct relevance to the ISIs encountered during burst discharge. At the beginning of a spike burst, ISIs were typically ~20 ms and shortened over several spikes to 3 - 7 ms. The ISI values during burst discharge are thus within the range which potentiate the DAP and produce a change in dendritic spike properties (Figs. 17,18). Moreover, the antidromic C-T intervals used to increase dendritic and somatic depolarizations experimentally were evoked with a constant antidromic ISI. One could expect these changes to be even more pronounced under normal conditions in which the ISI decreases with each spike in a burst.

Figure 15.

Somatic AHPs are stable during repetitive spike discharge. *A*, Schematic diagram of a pyramidal cell indicating a somatic recording site and repeated focal pressure ejections of TTX (10 μM) in the apical dendritic region to block dendritic spike discharge and the DAP. *B*, Current-evoked spike bursts prior to TTX ejection indicating an apparent change in both AHP and DAP amplitudes during spike bursts (bAHPs are denoted by arrows). Inset at right shows magnified and superimposed views of the first spike (narrow trace) and third spike (thick trace) of the indicated burst. *C*, Spike discharge and AHPs recorded immediately prior to TTX diffusion to the cell body layer, ensuring a complete block of backpropagating dendritic spikes and the DAP. Note the lack of change in AHP amplitudes when recorded in isolation of dendritic activity in *C*. Inset at right shows an expanded view of the first and third spikes of the indicated burst.

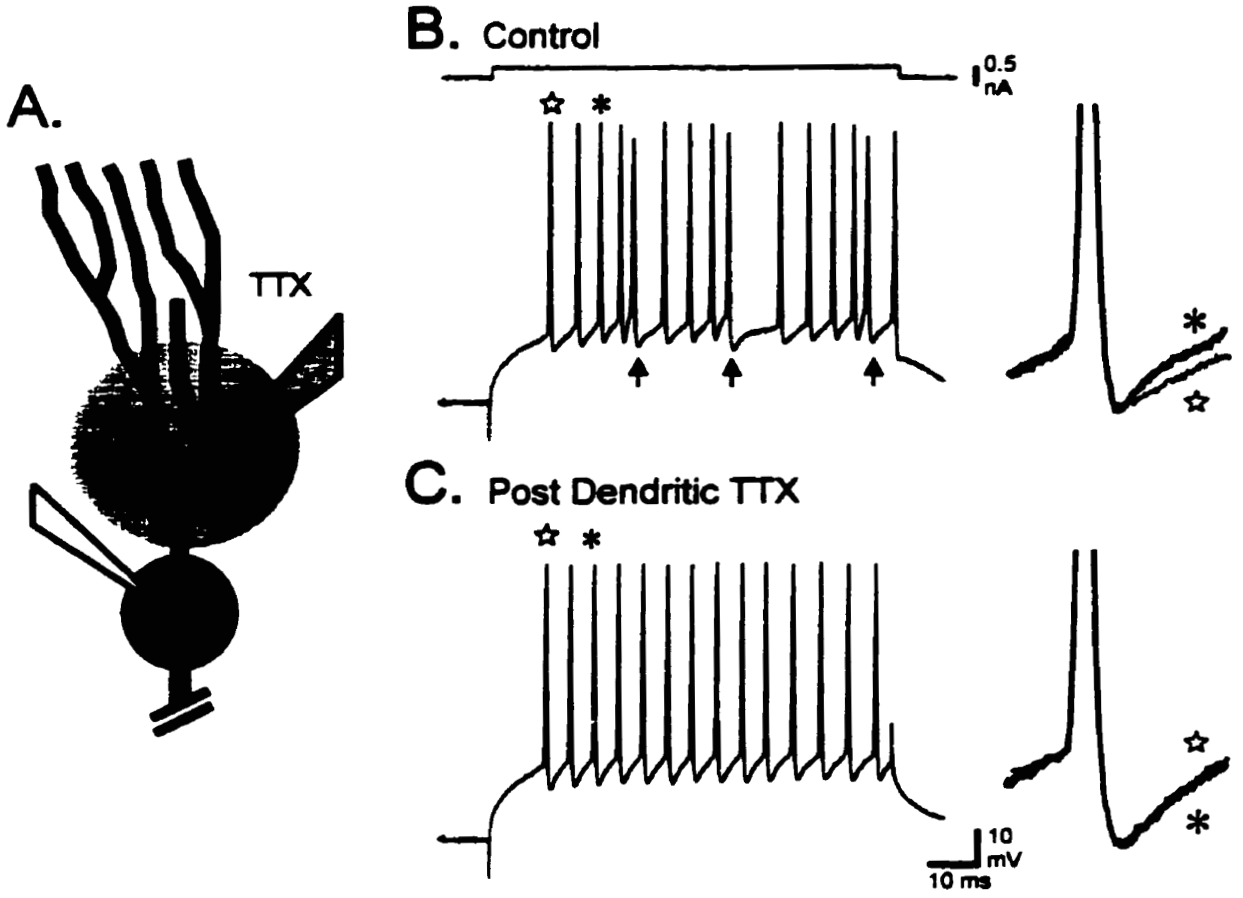
A.
TTX
B. Control
0.5
nA
C. Post Dendritic TTX
10
mV
10 ms

Figure 16.

Burst discharge selectively alters dendritic spikes. *A*, A somatic recording exhibiting several spike bursts in response to current injection (bAHPs denoted by arrows). Inset at right shows expanded and superimposed views of the first (thin trace) and third somatic spike (thick trace) in the indicated burst. Note the lack of change in spike repolarization and width during burst discharge. *B*, A dendritic recording illustrating current evoked spike bursts. In contrast to the soma, there is a substantial decrease in the rate of repolarization and increase in dendritic spike duration during a burst (inset at right superimposes the first (thin trace) and third dendritic spike (thick trace) in the indicated burst). *C,D*, Plots of the mean rate of spike repolarization (*C*) and spike width (*D*) during spike bursts in the recordings shown in *A* and *B* indicate a select and marked change in dendritic spike properties (** $p<.05$; *** $p<.001$ in comparison to controls; $n = 7$ somatic bursts, 8 dendritic bursts). Spike width was measured at a time corresponding to 10% of peak spike amplitude.

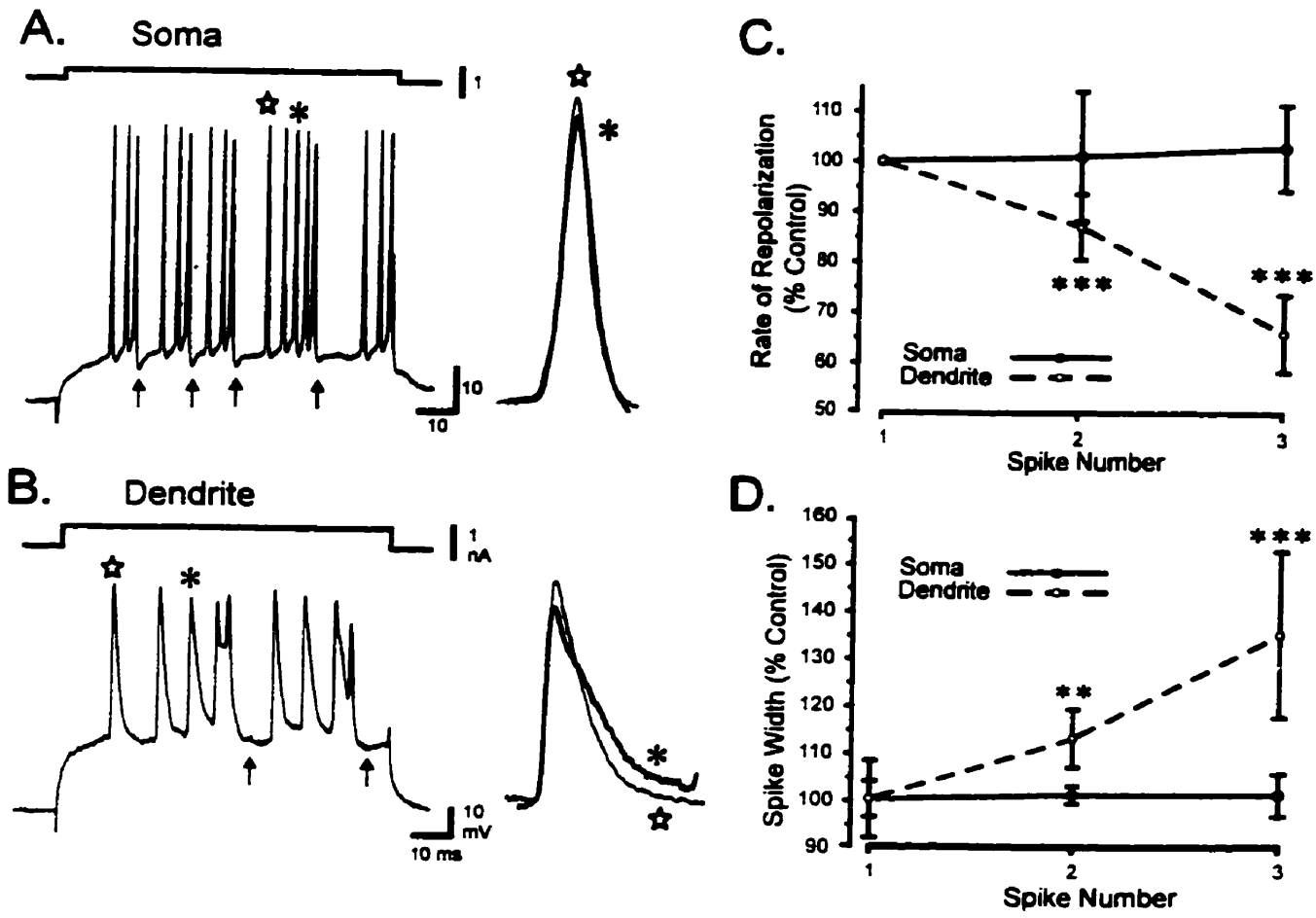
A.
Soma
1
10
10
B.
Dendrite
1
nA
10
mV
10 ms
C.
Rate of Repolarization
(% Control)
110
100
90
80
70
60
50
***
***
Soma
Dendrite
1
2
3
Spike Number
D.
Spike Width (% Control)
160
150
140
130
120
110
100
90
Soma
Dendrite
**
***
1
2
3
Spike Number

Figure 17.

The somatic DAP and dendritic spike depolarization exhibit frequency-dependent potentiation. *A,B,* A representative series of antidromic stimulus pairs delivered at the indicated condition-test (C-T) intervals. Insets show expanded and superimposed views of control (thin trace) and test (thick trace) responses. Stimulus artefacts were reduced for illustrative purposes. At the soma (*A*), a C-T interval of 3.0 ms selectively reduced DAP amplitude (middle traces). A C-T interval of 3.7 ms markedly potentiated the DAP, effectively triggering a spike doublet (lower traces, slanted arrows denote second spike; two sweeps superimposed). In an apical dendrite, C-T intervals of less than ~4.9 ms gradually reduced dendritic spike amplitude to a minimum at 3.7 ms C-T, revealing a small pre-potential reflected from the soma (middle traces). At a C-T interval of 4.7 ms the dendritic spike duration was increased and a spike doublet was triggered (arrows in lower trace denote second spike of pair). Dashed lines in the lower somatic and dendritic trace indicate the latency used to measure the absolute voltage at the estimated peak of the somatic DAP (latency of second evoked spike) shown in *C* and *D*. *C, D,* Plots of the absolute voltage of the somatic DAP and dendritic spike at varying antidromic C-T intervals. The latency for measurements was fixed at the estimated peak of the somatic DAP (*A* and *B,* dashed lines) . Note the close correspondence between the absolute voltage attained in dendritic recordings to that of somatic DAP amplitude, including a gradual reduction at shorter C-T intervals. Some increase in DAP amplitude and dendritic voltage can still be detected on test pulses at > 15 ms C-T intervals.

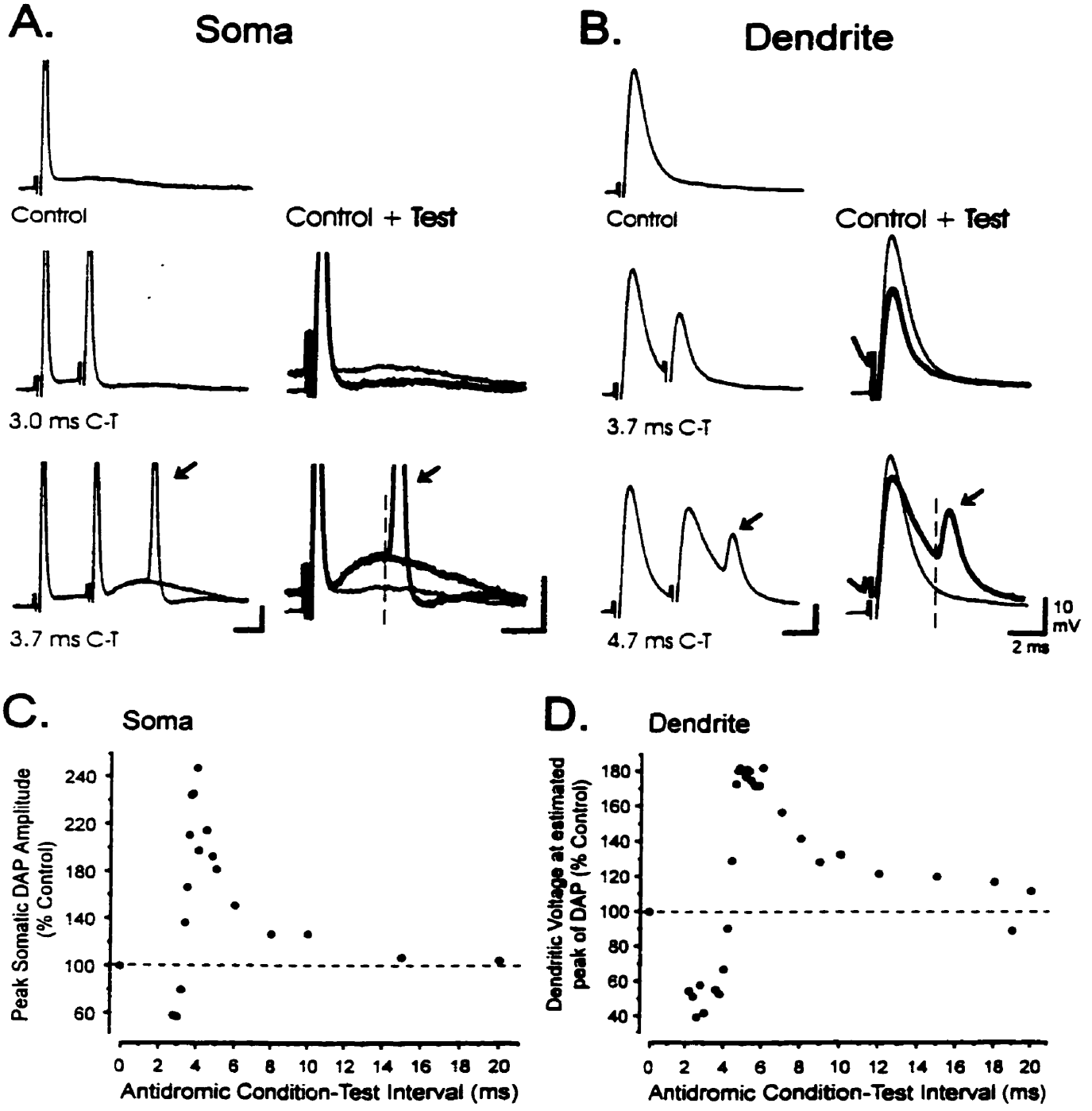
A.
Soma
Control
Control + Test
3.0 ms C-T
3.7 ms C-T
B.
Dendrite
Control
Control + Test
3.7 ms C-T
4.7 ms C-T
10 mV
2 ms
C.
Soma
Peak Somatic DAP Amplitude (% Control)
240
220
180
140
100
60
0 2 4 6 8 10 12 14 16 18 20
Antidromic Condition-Test Interval (ms)
D.
Dendrite
Dendritic Voltage at estimated peak of DAP (% Control)
180
160
140
120
100
80
60
40
0 2 4 6 8 10 12 14 16 18 20
Antidromic Condition-Test Interval (ms)

Figure 18.

Repetitive spike discharge summates dendritic spikes and lowers the threshold for burst generation. *A*, Superimposed records of antidromic dendritic and somatic spikes evoked singly or in 3-4 stimulus trains at an ISI that led to the generation of a spike doublet (slanted arrows; 6.0 ms ISI in dendrite, 9.1 ms ISI in soma). Note the summation of dendritic spikes, the increase in dendritic spike width and marked increase in DAP amplitude during a stimulus train. Dashed lines and double arrows indicate the estimated latency of the somatic DAP generating the second spike of the doublet for the plots shown in *B*. *B*, Plots of the absolute dendritic membrane potential (open circles) and DAP amplitude (closed circles) at the latencies shown in *A* with successive spikes in a stimulus train. *C,D*, Dendritic spike summation permits a lower ISI to trigger a spike doublet (defined as burst discharge) during repetitive activation. *C*, Two antidromic dendritic stimulus trains (two and six stimuli) illustrating the longest ISIs capable of triggering a spike doublet (arrows). *D*, Plot of the longest ISIs capable of evoking a spike doublet as the antidromic dendritic stimulus train in C was increased from 2 to 6 spikes. Lines in *B* and *D* represent best fit sigmoidal curves. Stimulus artifacts were reduced for illustrative purposes.

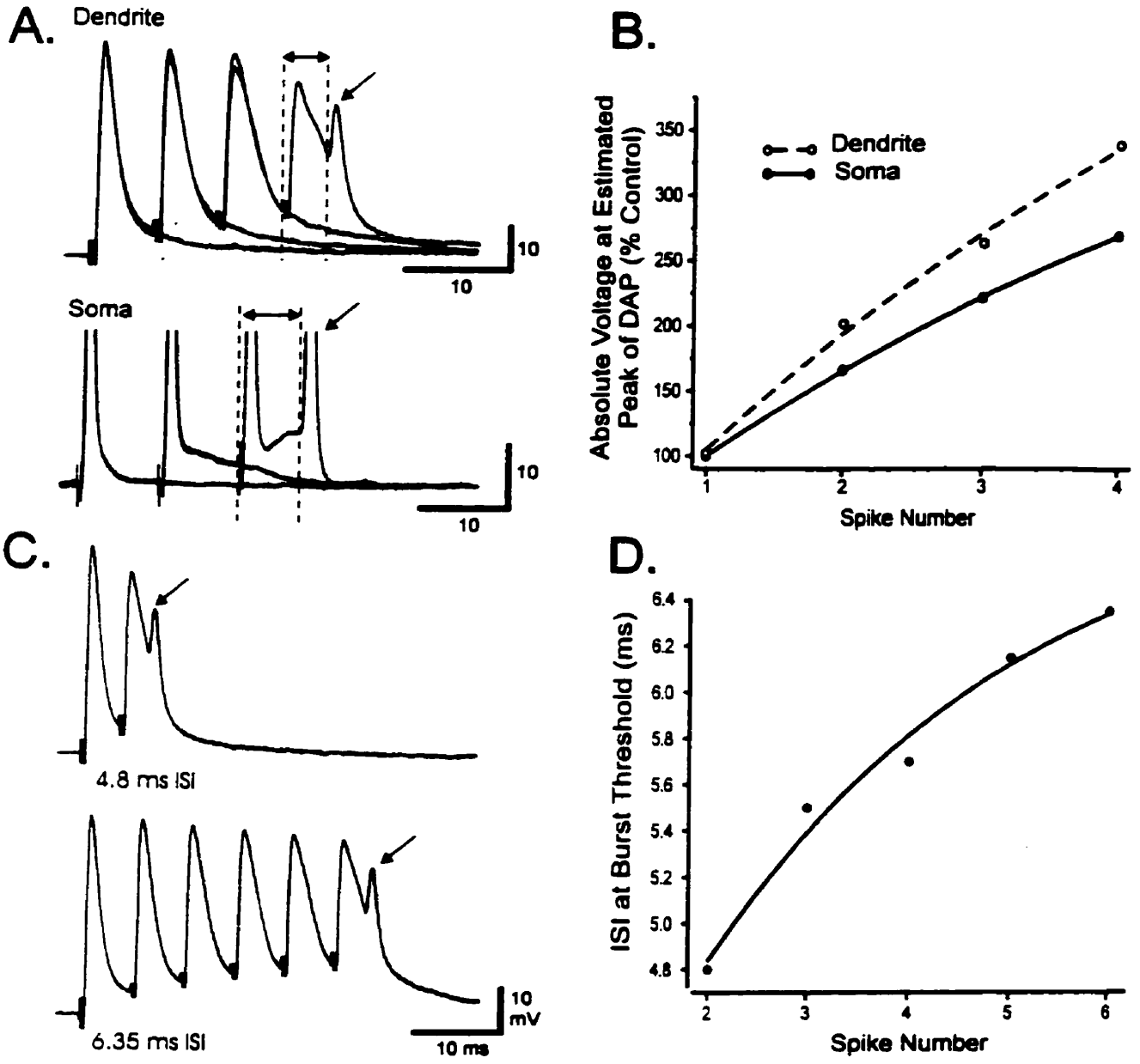
A.
Dendrite
10
10
Soma
10
10
B.
Absolute Voltage at Estimated Peak of DAP (% Control)
350
300
250
200
150
100
Dendrite
Soma
1
2
3
4
Spike Number
C.
4.8 ms ISI
6.35 ms ISI
10 mV
10 ms
D.
ISI at Burst Threshold (ms)
6.4
6.2
6.0
5.8
5.6
5.4
5.2
5.0
4.8
2
3
4
5
6
Spike Number

SPIKE DOUBLETS AND BURST TERMINATION

Since spike bursts end with a spike doublet and bAHP, the doublet may act to inhibit the soma-dendritic process underlying the burst. As indicated above, the second spike of the doublet in dendrites was only a small pre-potential, suggesting failure of the dendritic spike. In this regard, the antidromic condition-test experiments above revealed different refractory periods for somatic and dendritic spike discharge. The somatic refractory period consistently fell within 2.5 ± 0.64 ms (n = 13). The range of C-T intervals that defined dendritic spike refractory period was more difficult to identify given that dendritic spike amplitude decreased gradually as C-T intervals were reduced below ~10 ms. This would suggest a progressive block of several active sites in apical dendrites with differing sensitivities to paired stimulation. This is consistent with the demonstrated punctate distribution of Na^+ channels in pyramidal cell apical dendrites, and the recording of several TTX-sensitive dendritic responses (Turner et al., 1994). There was also some indication that the refractory period in dendrites increased with distance from the soma (data not shown). However, by defining the dendritic refractory period as the C-T interval evoking only a pre-potential of stable amplitude in recordings ≥ 100 μm from the soma, I arrived at a value of 4.5 ± 0.93 ms (n = 14).

The observed failure in dendrites of the second spike of a doublet may then result if the spike doublet ISI falls within the dendritic spike refractory period. To test this, I compared the spike doublet ISI recorded during current-evoked burst discharge to the refractory period measured with antidromic stimulus pairs in individual somatic and dendritic recordings. These experiments revealed that the ISI for spike doublets at the soma was consistently longer than the measured somatic spike refractory period (difference of

0.96 ± 0.78 ms; $n = 9$; $p < .01$; Wilcoxon Signed Ranks test), allowing two full amplitude action potentials to be generated (Fig. 19*A*,*B*). In contrast, the spike doublet ISI measured in dendritic recordings always fell within the range of antidromic C-T intervals that reduced dendritic spike amplitude, and within 0.4 ± 0.55 ms from the defined minimal refractory period (Fig. 19*C*,*D*; $p < .05$; Wilcoxon Signed Ranks test; $n = 8$).

I then tested whether a spike doublet could terminate a burst by simulating a spike doublet during an antidromic stimulus train (Fig. 20). This was accomplished by inserting an additional stimulus at varying latencies within an antidromic stimulus train of fixed ISI. In dendrites I found that the addition of an antidromic stimulus at latencies close to the dendritic refractory period produced only a small pre-potential on the falling phase of the previous spike (Fig. 20*A*). This blocked the discharge of at least one subsequent dendritic spike of the background stimulus train, presumably through the actions of a bAHP. In contrast, an additional stimulus inserted at longer latencies evoked nearly full sized dendritic spikes and no subsequent inhibition of spike discharge (data not shown). In somatic recordings, inserting an additional antidromic stimulus at effective C-T intervals of ~3 - 5 ms evoked a spike doublet comprised of two full spikes followed by inhibition of subsequent spike discharge (Fig. 20*B*). The use of C-T intervals near the somatic spike refractory period resulted in failure of the imposed spike but no interruption of spike discharge in response to subsequent stimuli in the train.

HYPOTHESIZED MECHANISM OF BURST GENERATION

I have developed a working hypothesis by which the frequency-dependence of spike broadening and dendritic spike conduction establish a process of "conditional backpropagation" to control burst discharge (Fig. 21). During repetitive spike discharge

at ISIs longer than ~8 ms, there is a faithful backpropagation of each spike from soma to dendrite. Spike ISIs of ~3-7 ms promote a selective broadening of dendritic spikes, allowing dendritic spikes to summate and exert a progressively greater influence on the soma as a DAP. As a result, the DAP increases in amplitude during a spike burst, ultimately reaching threshold to trigger a spike doublet at the soma. The spike doublet ISI is longer than the refractory period of the soma, allowing two full action potentials to be generated. The first of these spikes backpropagates into dendrites, but the second fails to backpropagate as it falls within the refractory period of dendritic spike discharge. This results in an abrupt loss of the dendritic depolarization driving the burst, allowing the membrane to repolarize in the form of a bAHP (Fig. 21). The absolute ISI capable of shifting a cell from tonic to burst output (ie burst threshold) varies according to the number of spikes discharged and the degree of dendritic spike summation.

Figure 19.

The spike doublet ISI falls within the refractory period of dendritic spikes. *A,B,* A somatic recording comparing the doublet ISI during current evoked burst discharge to the spike refractory period. *A,* An expanded view of a current evoked somatic spike burst, indicating a spike doublet ISI of 4.1 ms (linked arrows). *B,* Antidromic C-T stimulus pairs in this recording indicate a spike refractory period of 2.8 ms, as indicated by superimposition of two stimuli illustrating an all-or-none failure of spike discharge on the second stimulus. Note that the short somatic refractory period allows the spike doublet in *A* with an ISI of 4.1 ms to be evoked as two full spikes. *C,D,* Dendritic recording comparing the doublet ISI and dendritic spike refractory period. *C,* An expanded view of a current evoked dendritic spike burst exhibiting a spike doublet ISI of 3.5 ms (linked arrows). *D,* Antidromic C-T stimulus pairs in this dendritic recording indicate that a C-T interval of 3.5 ms falls within the refractory period of the dendritic spike, revealing the small pre-potential associated with somatic spike discharge (long arrow). Superimposition of antidromic test stimuli delivered at progressively longer C-T intervals illustrates an eventual return of test dendritic spikes to control spike amplitude. Antidromic stimulus artifacts were reduced for illustrative purposes.

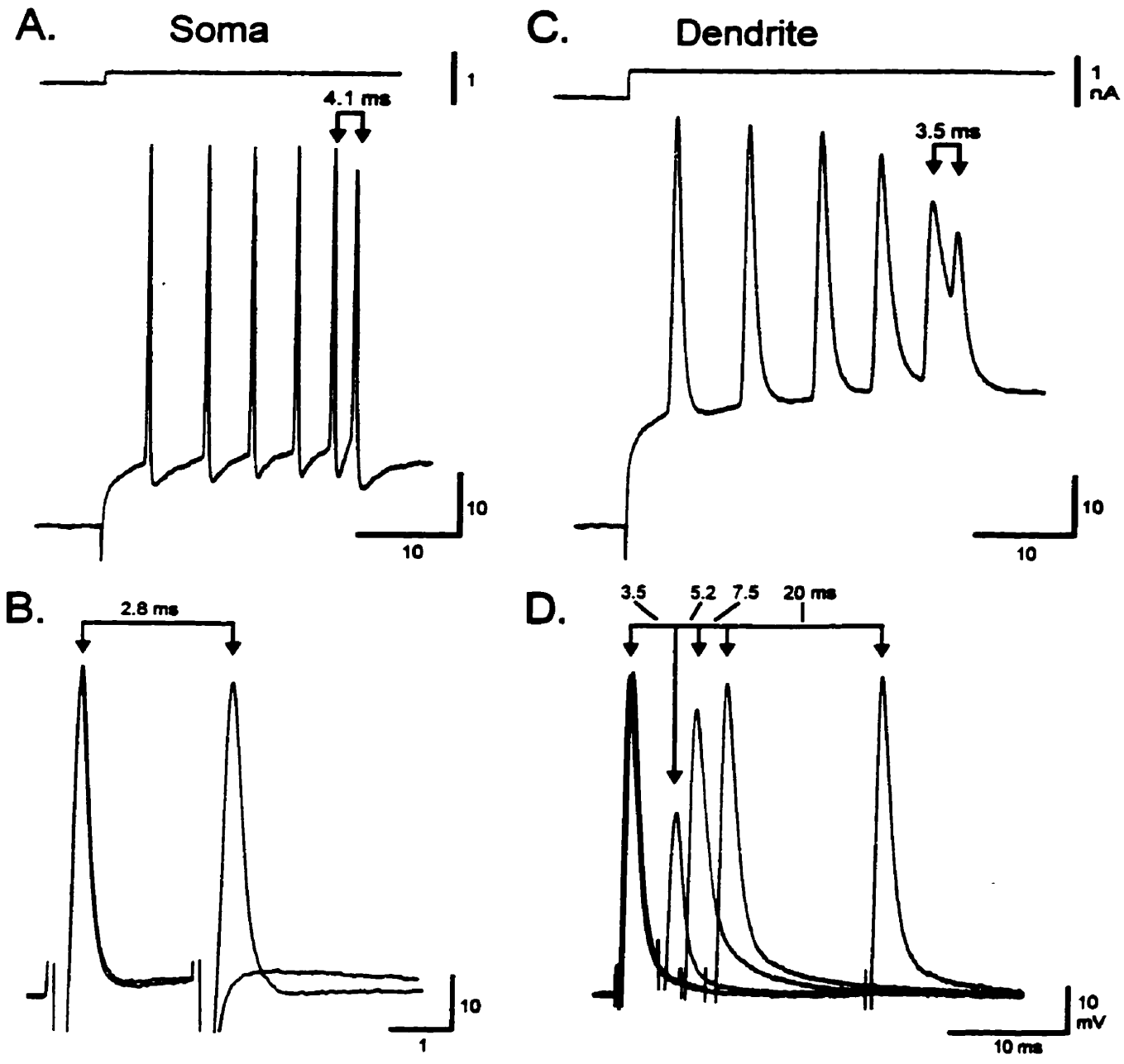
A.
Soma
1
4.1 ms
10
10
C.
Dendrite
1
nA
3.5 ms
10
10
B.
2.8 ms
10
1
D.
3.5
5.2
7.5
20 ms
10
mV
10 ms

Figure 20.

Invoking a spike doublet inhibits spike discharge and triggers a bAHP. *A*, Upper trace: A dendritic recording illustrating a train of 5 antidromic spikes (7.1 ms ISI). Lower trace: A spike doublet is simulated by inserting an additional antidromic stimulus 3.9 ms after the third spike in the train (linked solid arrows). The new stimulus fell within the refractory period of the dendritic spike, evoking only a small pre-potential (open arrow) and a subsequent bAHP capable of inhibiting discharge of the next spike in the train (slanted arrow). *B*, Upper trace: A somatic recording illustrating a train of 6 antidromic spikes (8 ms ISI). Lower trace: A spike doublet is simulated by inserting an additional antidromic stimulus (open arrow) 3.6 ms after the fourth spike in the train. This evoked a full spike at the soma, but also inhibited subsequent spikes in the stimulus train (solid arrows indicate a pre-potential signifying failure of the somatic spike). Antidromic stimulus artifacts are reduced for illustrative purposes.

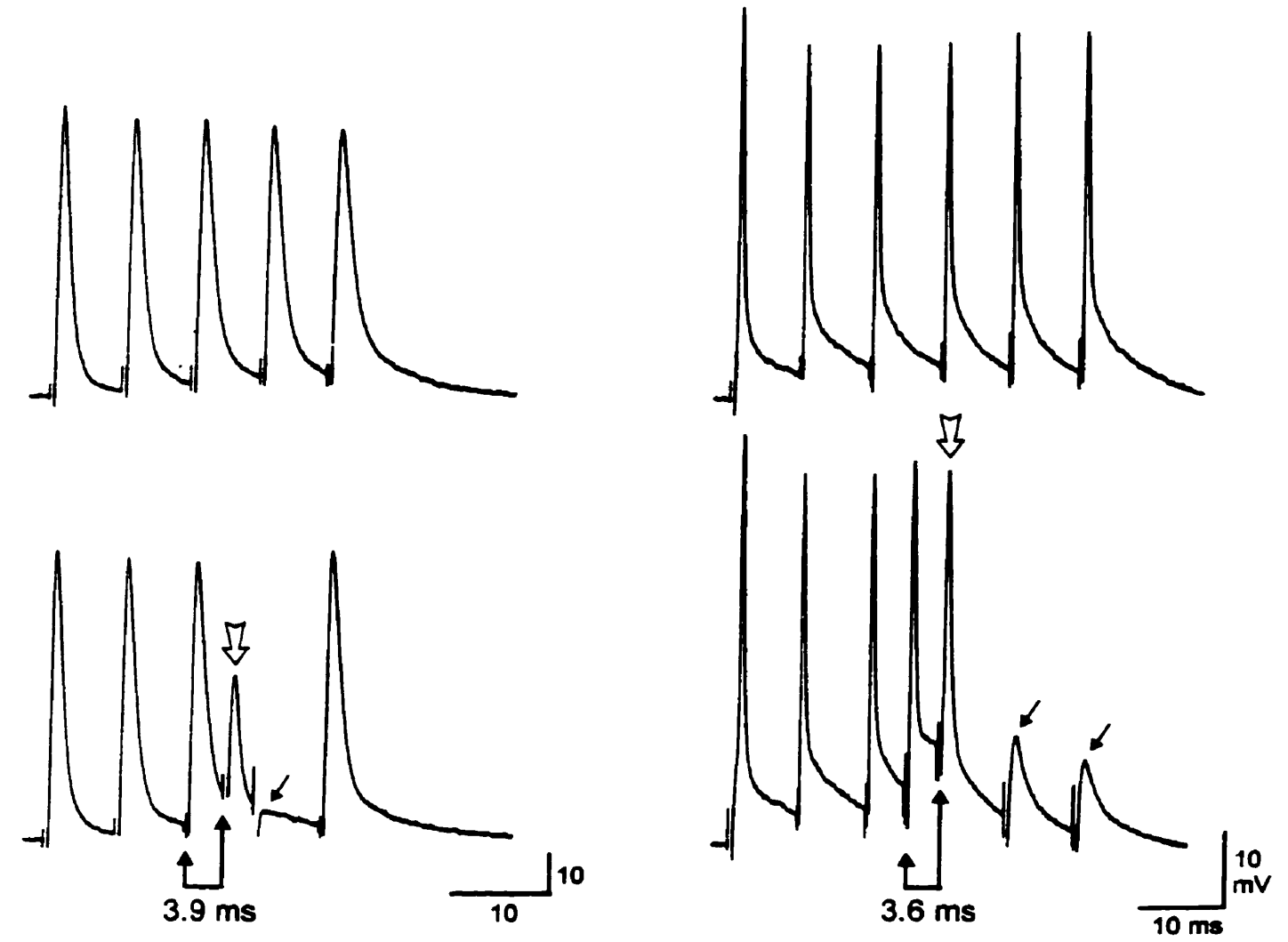
A. Dendrite
B. Soma
3.9 ms
10
10
3.6 ms
10
mV
10 ms

Figure 21.

Working hypothesis of how conditional backpropagation controls burst discharge. *A,B,* Representative spike bursts in a pyramidal cell dendrite and soma. The records in *A* depict the somatic contribution to dendritic activity during a burst, while records in *B* illustrate the dendritic contribution to somatic depolarization during a burst. The weight of influence is shown by the size and shading of arrows. *A,* Each successive somatic spike in a burst triggers a full spike capable of backpropagating into dendrites. *B,* Each successive dendritic spike in a burst is longer in duration than the last, progressively increasing current flow back to the soma (shaded arrows). There is a concurrent increase in DAP amplitude and duration until the DAP becomes large enough to reach threshold to trigger a spike doublet at the soma. The short ISI of the spike doublet (3.0 ms) falls at or within the refractory period of dendritic membrane (4.5 ms), preventing backpropagation of the second spike of the pair. This failure of dendritic spike discharge eliminates the dendritic depolarization driving the spike burst (denoted by dashed arrow). A subsequent bAHP repolarizes the cell membrane.

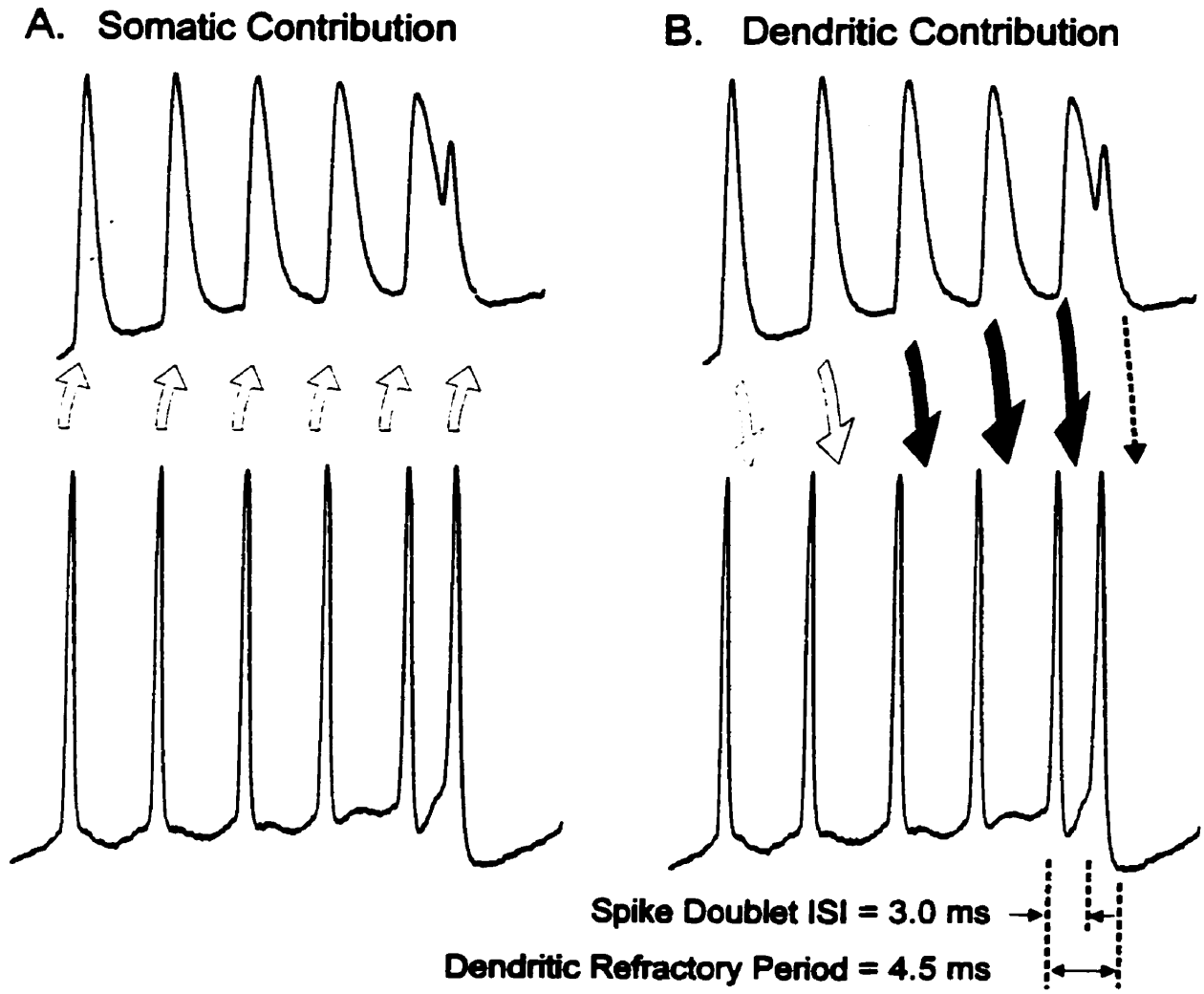
A. Somatic Contribution
B. Dendritic Contribution
Spike Doublet ISI = 3.0 ms
Dendritic Refractory Period = 4.5 ms

CHAPTER 4

DISCUSSION

The present study describes a novel mechanism by which a conditional backpropagation of Na^+ spikes controls oscillatory spike bursts in a central neuron. Burst discharge is dependent upon the generation of a DAP at the soma by a dendritic Na^+ spike backpropagating from the soma. The ELL pyramidal neuron has a length constant (λ) of 550 μM. A dendritic recording site 200 μM from the soma is therefore at only .36 of λ. By comparison the dendritic spike can thus be expected to discharge nearly simultaneously with the somatic spike. This makes the largest effect of the dendritic spike on the somatic membrane potential not visible. The somatic DAP is closely related to the falling phase of the dendritic spike. I have now shown that backpropagating spikes undergo a frequency-dependent broadening that enhances dendritic spike summation and potentiates the somatic DAP during a burst. The eventual generation of a somatic spike doublet abruptly terminates burst discharge when the relatively long refractory period of dendritic membrane prevents backpropagation of the second spike of the doublet. Thus, a process of conditional backpropagation regulates dendritic spike invasion to alternately drive or terminate a spike burst, providing extensive control over the threshold and frequency of oscillatory discharge.

The potential for dendritic spikes to secondarily depolarize somatic membrane was raised in some of the earliest reports of intracellular recordings (Granit et al., 1963; Nelson and Burke, 1967; Calvin and Sypert, 1976; Calvin and Hartline, 1977). Interactions between a backpropagating spike and a somatic DAP have been suggested more recently

in cortical pyramidal cells, although this also involved activation of dendritic Ca^{2+} currents (Zhang et al., 1993; Mainen and Sejnowski, 1996; Golding et al., 1999; Magee and Caruth, 1999). Turner et al. (1994) established the relevance of this mechanism in ELL pyramidal cells, and I have now shown how conditional backpropagation of dendritic Na^{+} spikes controls burst discharge. Importantly, spike doublets have been reported in several bursting cell types ranging from receptors to cortical pyramidal cells, but their role in burst discharge has not been established (Granit et al., 1963; Nelson and Burke, 1967; Calvin and Sypert, 1976; Calvin and Hartline, 1977; Steriade et al., 1993; Paré et al., 1995; Gray and McCormick, 1996; Koch, 1999). The mechanism I describe for spike doublets in ELL pyramidal cells may then prove to be a common strategy for controlling burst output.

FAST OSCILLATIONS IN ELL PYRAMIDAL CELLS

In 60% of ELL pyramidal cells studied there was a clear threshold for burst discharge observed on the F/I curve. For the remaining 40% of the cells, increased depolarizing current injection increased the tonic firing frequency without inducing a shift to burst discharge. The question remains as to why 40% of the cells recorded from did not exhibit burst discharge. One reason may be that the level of current injection necessary to shift some of these cells from tonic to burst firing was not reached. This seems to be an unlikely explanation for many cells, as several of the non-bursting cells continued to fire tonically despite large (> 1 nA) depolarizing current steps. A second explanation could be a difference between basilar and non-basilar pyramidal cells discharge properties. This might also account for the occurrence of two peak distributions of oscillatory

frequency obtained at the highest levels of current injection during construction of F/I curves (Fig. 7*C*).

Variance in cell morphology could also explain the differential ability of ELL pyramidal cells to fire spike bursts. The dependence of burst firing on cell structure is supported by the finding that oscillation frequencies at the high end of the F/I curve were represented by two populations of cells (Fig.7*C*). Mainen and Sejnowski (1996) demonstrated that the ability of pyramidal cells to burst could be completely explained by their dendritic morphology. Using a computer model of a neocortical pyramidal cell with a uniform distribution of Na^+ and K^+ channels in soma and dendrite, Mainen et al. (1996) showed that cells with larger dendritic trees were capable of oscillatory discharge, while cells with smaller dendritic trees only fired tonically. The underlying mechanism for this was that further backpropagation into the dendritic tree in their model promoted the generation of a larger DAP at the soma.

The possible role of dendritic morphology in burst discharge in the ELL is supported by anatomical studies which show a wide range of dendritic area among basilar pyramidal cells (Bastain and Courtright, 1991). Bastian and Courtright (1991) found that an ELL basilar pyramidal cell's dendritic morphology corresponded to the cell's firing pattern *in vivo* in response to sensory stimulation. Pyramidal cells with small apical dendrites were shown to fire more regularly and with a higher frequency, while cells with larger apical dendrites fired brief bursts of action potentials separated by long intervals. Bastian thought that this difference in firing pattern might be due to an increased level of GABAergic stellate cell input to the phasic cell types with larger apical dendritic trees. My research would now suggest that the correspondence of the cell's firing pattern to

dendritic morphology may be due to a differential degree of spike backpropagation. Pyramidal cells with larger dendritic trees may receive more depolarizing current at the soma from backpropagating dendritic spikes, and therefore be more likely to exhibit burst discharge. Conversely, it may well be that some of the 40% of cells not exhibiting burst discharge had their dendritic trees truncated during the ELL slice preparation and were therefore left incapable of firing spike bursts.

FACTORS CONTROLING BURST DEPOLARIZATIONS

Extensive work in other cells exhibiting burst discharge has identified several key elements that can contribute to the depolarization that drives spike bursts. Several currents have been implicated in this depolarization, including the interaction between I_h and I_T as well as conductances from I_{Ca}, I_{NaP}, I_{NaS}, $I_{Cl(Ca)}$. Synaptic EPSPs have also been shown to contribute to the generation of DAPs in some cells. I consider each of these factors as potential contributors to the DAP below.

I_h and I_T

In many cells, burst frequency is controlled by the magnitude of Ca^{2+} influx invoked during the burst depolarization, where there is an associated increase of Ca^{2+} current with each Na^+ spike (Aldrich et al., 1979; Bourque, 1991; Jackson et al., 1991; Quattrocki et al., 1994; Ma and Koester, 1995; Klemic et al., 1998; Borst and Sakmann, 1999). Calcium influx can be directly linked to the size of the depolarization, the number of Na^+ spikes generated, or burst duration. These factors may be directly linked to the duration and amplitude of the bAHP, and therefore oscillation frequency (Hotson and Prince, 1980; McCormick and Pape, 1990). In other cells, a Ca^{2+}-dependent depolariza-

tion drives the burst while a Ca^{2+}-dependent hyperpolarization repolarizes the cell to it's resting membrane potential (Lewis, 1984). A similar result occurs in thalamic neurons through a voltage-dependent inactivation of T-type Ca^{2+} currents during the burst. This acts to control the burst duration, with faster inactivation of the T-type Ca^{2+} current shortening burst duration and increasing oscillatory frequency. The time-course of the subsequent AHP in each of these cases can also depend on the time-course for recovery from deactivation of an inwardly rectifying current I_h (McCormick and Huguenard, 1992).

Importantly, neither I_T nor I_h are expected to contribute to fast burst discharge in CMS pyramidal cells, as whole cell voltage clamp recordings at the soma in the presence of TTX reveals little or no inward Ca^{2+} current, and no I_h during membrane step hyperpolarizations from –60 to -120 mV (E. Morales, personal communication).

Generation of the DAP

I_{Ca}

Inward Ca^{2+} currents have been shown to underlie depolarizations during burst discharge in several cell types. A Ca^{2+} current was found to underlie DAPs in magnocellular neurosecretory cells (Bourque, 1986) and supraoptic neurones (Bourque et al. 1986). The DAP and burst generation in CA3 pyramidal cells are believed to be mediated primarily by a slow Ca^{2+} current (Johnston et al. 1980; Hotson and Prince, 1980). A T-type Ca^{2+} current is apparent in the cat and rat lateral geniculate nucleus and contributes to a depolarization during burst activity (Crunelli et al. 1989). A Ca^{2+} dependent current has also been shown to mediate a DAP that is involved in the generation of spike bursts in

cortical pyramidal cells (Kang and Ohmori, 1999) and hippocampal CA1 pyramidal cells (Azouz et al. 1996) *in vitro*.

I_{Ca} however does not appear to contribute substantially to DAP generation in CMS pyramidal cells, as experiments using focal somatic (n=6) and dendritic Cd^{2+} (n=3) ejections have shown no apparent modulation in burst discharge (data not shown). As indicated above whole cell voltage clamp recordings at the soma in reveal little or no Ca^{2+} current. An inward dendritic Ca^{2+} current may however play a role in depolarizing the cell during burst discharge.

I_{NaP} and I_{NaS}

I_{NaP} could well contribute to the DAP, but its role in DAP generation is hard to assess given the difficulty of selectively blocking it. In a model based on the mechanism for burst discharge described by Turner et al. (1994), Wang (1999) showed that I_{NaP} was sufficient to produce burst discharge in visual cortical pyramidal cells even without active dendritic spike backpropagation. However, there are differences between the form of bursting in Wang's model and the burst discharge seen in ELL pyramidal cells. In Wang's model a large DAP is generated at the end of a burst which is not seen in ELL pyramidal cells. Furthermore, focal dendritic ejection of TTX blocks spike bursts in ELL pyramidal cells, revealing a dependence on active spike backpropagation. Nevertheless I_{NaP} can not be ruled out as a possible factor modifying DAP amplitude as current is conducted from the dendrite to the soma. A slow TTX-insensitive Na^+ current (I_{NaS}) has also been found to contribute to DAPs in CA1 pyramidal neurons (Hoehn et al. 1993). A slow Na^+ dependent pre-potential does exist in CMS pyramidal cells, but this has been shown

to be entirely blocked by TTX. Therefore a TTX-insensitive I_{NaS} does not likely play much of a role in DAP generation in ELL pyramidal cells.

$I_{Cl(Ca)}$

DAPs may also be mediated by activation of Ca^{2+} activated Cl^- channels. A $I_{Cl(Ca)}$ contributes to DAP generation in lateral amygdala neurons (Sugita et al., 1993), cultured spinal (Owen et al., 1986) or sensory neurons (Mayer, 1985; Scott et al., 1988), parasympathetic neurons (Akusa et al., 1990; Tokimas et al., 1988), and cingulate cortical neurons (Higashi, 1993). Any affect of $I_{Cl(Ca)}$ in generating the DAP in ELL pyramidal cells would be minute as there is very little Ca^{2+} current at the soma. In addition, since GABAergic Cl^- - dependent IPSPs reverse at ~ -70 mV in ELL pyramidal cells (Berman and Maler, 1998), a reversal in the Cl^- gradient at the soma can be ruled out as a contributing inward current to DAP generation.

Synaptic (EPSPs)

In the hippocampus, networks of synaptically connected inhibitory interneurons can generate gamma oscillations; the same frequency range as ELL pyramidal cells (Whittington et al. 1995). Indeed, computer simulations of several parts of the brain suggest that gamma oscillations can be generated by pools of excitatory neurons, networks of inhibitory neurons, or networks of excitatory and inhibitory neurons (Jefferys et al. 1996). Eeckman and Freeman (1990) demonstrated in the rat olfactory cortex that short range negative feedback interactions between cortical pyramidal and granule cells were sufficient to induce bursting. This recurrent inhibitory loop which generated burst discharge involved $GABA_A$ receptor-mediated synaptic potentials. Berman and Maler (1998) found that ELL pyramidal cells have both $GABA_A$ and $GABA_B$ receptors. How-

ever, a recurrent inhibitory loop can be ruled out for generating burst discharge in ELL pyramidal cells as they do not extend any axonal recurrent collaterals (Maler et al. 1981). ELL pyramidal cells thus appear to be intrinsically bursting neurons.

Frequency-dependent spike broadening

The frequency-dependent broadening and enhanced summation of dendritic spikes results in a parallel increase in the absolute dendritic voltage and DAP amplitude with each successive spike in a burst. This process is maximal for ISIs between 3 - 7 ms and controls burst threshold by regulating the transition from tonic to burst output (Figs. 2 and 3). The exact spike frequency capable of reaching this transition point depends on the number of spikes invoking dendritic spike summation (Fig. 10*C,D*). As a result, the immediate history of spike discharge can influence burst threshold. I would thus expect burst output to begin at even longer ISIs during the spontaneous activity found *in vivo* (Gabbiani et al., 1996).

Frequency-dependent spike broadening has been reported in cell bodies, axons, and presynaptic terminals of several cell types (Aldrich et al., 1979; Bourque, 1991; Jackson et al., 1991; Quattrocki et al., 1994; Ma and Koester, 1995; Mathes et al., 1997). This most often involves a cumulative inactivation of A-type or delayed rectifying K^+ currents underlying spike repolarization (Aldrich et al., 1979; Jackson et al., 1991; Quattrocki et al., 1994; Ma and Koester, 1995; Klemic et al., 1998; Tkatch et al., 1999), and an associated increase of Ca^{2+} current activated by the Na^+ spike (Aldrich et al., 1979; Bourque and Renaud, 1985; Bourque, 1991; Jackson et al., 1991; Ma and Koester, 1995; Borst and Sakmann, 1999). In CA1 pyramidal cells, inactivation of a BK-type Ca^{2+}-dependent K^+ channel was recently reported to contribute to frequency dependent spike

broadening (Halvorsrud et al., 1999). Backpropagating Na^+ spikes can also activate dendritic Ca^{2+} currents in a manner dependent on spike frequency and conduction along the dendritic axis (Jaffe et al., 1992; Spruston et al., 1995; Callaway and Ross, 1995; Larkum et al., 1996, 1999). The precise role for Ca^{2+} currents in spike broadening in ELL pyramidal cell dendrites is presently unknown. However, focal dendritic Cd^{2+} ejections (200 μM) have little effect on dendritic activity in CMS pyramidal cells (n = 6; Lemon and Turner, unpublished observations). Dendritic spike broadening thus appears to result primarily from actions on TTX-sensitive dendritic Na^+ spikes.

The reason repetitive discharge induces a selective change in dendritic spike repolarization has not been determined, but could relate to K^+ channel density, K^+ channel subtypes, or their inactivation by the very different action potential waveforms in somatic versus dendritic regions. A current hypothesis centers upon the potential role of a gymnotid homologue of the mammalian Kv3.3 channel (AptKv3.3) that has been localized to both somatic and dendritic membranes (Rashid and Dunn, 1998a,b; Morales et al., 1998). This channel is similar in properties to the Kv3.1 channel in exhibiting a high threshold (-20 mV) for activation. This allows the channel to repolarize action potentials and set the maximal frequency of spike discharge in a variety of cell types (Kanemsa et al. 1995, Brew and Forsythe, 1995; Perney and Kaczmarek, 1997; Massengil et al., 1997; Martina et al., 1998; Hernandez-Pineda et al., 1999).

Significantly, dendritic spikes in pyramidal cells peak at ~ 0 mV, indicating that AptKv3-like current in dendritic regions would be just activated by a dendritic spike. During burst discharge dendritic spike amplitude decreases in a progressive and fre-

quency-dependent manner (Fig. 19). This decline in dendritic spike amplitude during spike bursts may be due to a cumulative inactivation of dendritic Na^+ channels, as found in hippocampal and cortical pyramidal cells (Fleidervish et al., 1996; Colbert et al., 1997; Mickus et al., 1999; Sourdet et al. 1999). The decline in dendritic spike amplitude due to Na^+ channel inactivation may then progressively decrease the activation of the AptKv3.3 channels, resulting in dendritic spike broadening.

In rat subicular neurons low concentrations of the K^+ channel blocker 4-AP converts spike discharge from regular spiking to repetitive bursting because it uncovers a Ca^{2+} current (Jung et al., 1999). Local application of 4-AP to the distal apical dendrites of CA1 pyramidal neurons also switches cell firing during a current-evoked depolarization from single to multiple spikes riding on a DAP (Carruth et al., 1999;Magee and Carruth, 1999). Focal dendritic ejection of TEA has also been shown to lower burst threshold in ELL pyramidal cells (Lemon, unpublished observation). This suggests that K^+ channel inactivation in apical dendrites underlies dendritic spike broadening, which serves to control burst threshold in ELL pyramidal cells.

Joho et al. (1999) recently demonstrated that a Kv3.1 knockout mouse exhibited enhanced gamma frequency oscillatory discharge. A decrease in AptKv3.3 channel activity in dendritic regions would increase the rate of spike broadening and the frequency of gamma bursts. The 40% of ELL pyramidal cells not exhibiting oscillatory discharge may therefore have a larger dendritic distribution of Kv3-type channels, preventing dendritic spike broadening and oscillatory discharge.

Role of Spike Doublets

The generation of a high frequency somatic spike doublet provides an intrinsic mechanism to terminate a spike burst. This results from the longer dendritic spike refractory period preventing backpropagation of the second spike of the doublet. The sudden loss of dendritic depolarization driving the burst then allows the cell to repolarize. The spike doublet is also significant in allowing the rate of dendritic spike summation and DAP potentiation to control burst frequency (Fig. 6).

Repetitive discharge in other cells has been shown to decrease dendritic spike amplitude to the point where backpropagating spikes fail to invade some distal dendritic branch points (Spruston et al., 1995; Colbert et al., 1997). Synaptic inhibition can also regulate the degree of spike backpropagation (Buzsaki et al., 1996; Tsubokawa and Ross, 1996). However, the mechanism I describe here differs substantially from these in representing an all-or-none failure of dendritic spike invasion at the level of proximal apical dendrites from one spike to the next. To my knowledge this is the first report of how dendritic refractory period regulates spike activity.

The exact location of dendritic spike failure can not be identified. However, I recorded dendritic spike failure in locations as close as ~50 μm from the cell layer, suggesting that dendritic refractory period increases at a minimal distance from the soma. The difference in somatic and dendritic spike refractory periods may result if dendritic spikes are generated by a comparatively low density of Na^+ and K^+ channels. Indeed, the eventual failure of dendritic spike discharge is likely augmented by an inactivation of dendritic Na^+ channels during a burst. Dendritic spike failure would become even more likely if cumulative inactivation of dendritic K^+ channels during a burst lengthened the

dendritic spike refractory period. An increase in somatic spike refractory period has in fact been shown by Massengill et al. (1997) in layer IV cortical neurons in response to TEA application. In this regard, I have preliminary data indicating that focal ejections of 5 mM TEA in the dendrite increases the refractory period in ELL pyramidal cell somata from 2.8 to > 5 ms (n = 1). The progressive increase in dendritic spike width during a burst may then increase dendritic refractory period from one spike to the next. Such a process would only serve to enhance the ability of a spike doublet to block invasion of the dendritic arbor. This may partly account for why the past history of cell discharge can act to regulate burst threshold. Figure 18(*C,D*) shows how an increasing number of preceding spikes in a train of action potentials can increase the ISI capable of generating burst discharge from 4.8 to 6.35 ms. This result may reflect a comparatively long dendritic refractory period when the number of spikes in a train are increased.

Generation of the bAHP

The spike doublet-induced failure of backpropagation was followed by a bAHP that prevented further spike discharge. Although the bAHP was not a primary focus of this study, it exhibited some unusual attributes with respect to burst generation. Most importantly, it was not clearly correlated with any aspect of burst discharge except for the preceding generation of a spike doublet. I am uncertain at this time as to whether a spike doublet is involved in generating the bAHP, or simply unmasks a bAHP when the dendritic spike depolarization is suddenly removed.

Many researchers have found long duration AHPs to be generated by Ca^{2+}- gated K^+ channels corresponding to $SK_{(Ca)}$, $BK_{(Ca)}$ or $IK_{(Ca)}$ channels, having small, large and intermediate conductances, respectively. An I_{AHP} underlying a sAHP in rat sympathetic

neurons is mediated by Apamin-sensitive $SK_{(Ca)}$ channels (Sacchi et al.1995). ELL pyramidal cells are insensitive to the $SK_{(Ca)}$ channel blocker Apamin, making $SK_{(Ca)}$ channels unlikely candidates for generating the bAHP. There is a good possibility however, that an intermediate conductance $IK_{(Ca)}$ or a large conductance $BK_{(Ca)}$ is responsible for generating the bAHP in ELL pyramidal cells. In support of this, E. Morales has recorded large conductance (180 pS) Ca^{2+}-sensitive K^+ channels sensitive to Iberiotoxin (20 nM) in both pyramidal cell somatic and dendritic membranes which are consistent with $BK_{(Ca)}$ channels (personal communication). Morales has also recorded an intermediate conductance (90 pS) Ca^{2+}-sensitive K^+ current in both soma and dendrites. Both of these $K_{(Ca)}$ conductances could thus play a role in generating the bAHP.

Jaffe et al. (1992) found that Ca^{2+} entry into dendrites of hippocampal pyramidal cells is triggered by Na^+ spikes that actively invade the dendrites. This Ca^{2+} entry generates a sAHP by an $I_{K(Ca)}$ termed I_{AHP}. In bullfrog ganglion neurons the time course of an I_{AHP} evoked by action potentials is a function of the Ca^{2+} load induced by the action potential (Goh and Pennefather, 1987). A Na^+ spike-induced Ca^{2+} entry in ELL pyramidal cell apical dendrites may then activate a K^+ conductance which could underlie the sAHP and/or the bAHP. The role of I_{AHP} in bAHP generation in ELL pyramidal cells is unknown, but my interpretation is that dendritic $I_{K(Ca)}$ will be more important than somatic $I_{K(Ca)}$ in generating the bAHP because:

(1) There is little inward Ca^{2+} current in CMS pyramidal cell somata (E. Morales and R.W. Turner, unpublished observations).

(2) Focal ejections of Cd^{2+} at the soma rapidly block the somatic sAHP, revealing a pronounced DAP of up to 100 ms at the soma, but leave the bAHP intact (data not shown).

(3) Focal ejections of Cd^{2+} to dendrites reduces the bAHP following a train of four antidromic spikes (data not shown).

Taken together these data suggest that Na^{+} spike induced Ca^{2+} entry in dendrites, particularly during the spike doublet may trigger Ca^{2+} activated K^{+} currents and therefore the bAHP. It remains to be determined, however, why focal dendritic Cd^{2+} ejections have little effect on dendritic spikes (n = 2).

An alternate explanation to bAHP generation can be seen in mammalian cortical neurons (Dryer, 1994). Dryer found a slow AHP to persist even when Ca^{2+} influx was blocked. This slow AHP was generated by a sodium activated potassium current (I $K_{(Na)}$). $IK_{(Na)}$ channels require relatively high concentrations of Na^{+} (in the order of 10-30 mM) for activation. It could well be that the bAHP is generated by a Na^{+} influx as can only be accumulated by a spike doublet. This would generate a similar afterhyperpolarization as the I $K_{(Na)}$ induced slow AHP.

Finally, an extremely interesting aspect of the bAHP was its almost all-or-none character after the triggering of a spike doublet. This might speak towards a mechanism not determined by voltage dependent ion channels, but perhaps by the passive membrane properties of the cell. In this scenario, the bAHP could simply represent a passive return of the membrane potential to rest when the dendritic depolarization is suddenly blocked. A similar mechanism in fact takes place in thalamic pacemaking cells, where inactivation of I_T and deactivation of I_h during a burst results in an abrupt return of membrane poten-

tial back to rest, thereby terminating spike bursts (McCormick and Pape, 1990). In support of this Morales has found evidence for inward rectifying channels in dendrites (personal communication), as has been reported in dendrites of hippocampal CA1 cells (Magee, 1998). Further work clearly needs to be done to discern the exact mechanism underlying bAHP generation. The most likely candidates for bAHP generation however appear to be a dendritic $BK_{(Ca)}$, $IK_{(Ca)}$ or $IK_{(Na)}$ conductance or a passive return of the membrane potential to rest.

SIGNIFICANCE OF FAST OSCILLATORY DISCHARGE

Apteronotus leptorhynchus can alter its EOD frequency in response to jamming signals created by the EOD of neighboring fish. This jamming avoidance response (JAR), can provide a seperation of EOD frequencies among neighboring fish that is required for accurate location of objects (Heilligenberg, 1991). Using selective ibotenic lesions *in vivo*, Metzner and Juranek (1997) showed that CMS is both necessary and sufficient for producing the JAR in both the *Apteronotus leptorhynchus* and in *Eigenmannia virescens*. Lesions to the CLS and LS in *Eigenmannia* and lesions to the LS in *Apteronotus* had no effect on the JAR (Metzner and Juranek, 1997). Pyramidal cells in the CMS have a smaller receptive field size and thus show higher spatial resolution than those in the LS (Shumway, 1989, Turner et al., 1996). This high temporal resolution would also be required for the computational mechanisms controlling the JAR (Heiligenberg, 1991).

Gabbiani et al. (1996) recorded fast oscillatory spike bursts in pyramidal cells *in vivo* in relationship to sensory activation. They found that pyramidal cells reliably encode the up and down strokes of electric field AMs through the generation of burst dis-

charge; identifying a role for burst discharge in feature extraction. These authors also tested the role for burst discharge in differentially encoding AM frequencies across the sensory maps in the related gymnotiform *Eigenmannia* (Metzner et al., 1998). This study failed to establish such a relationship, although the final conclusions to be drawn from these experiments are in doubt due to several confounding factors (ie. species, choice of anesthetic, method of AM stimulation compared to Shumway (1989)). These studies are now being repeated with more attention to these factors to more convincingly test this hypothesis. Regardless, the important demonstration that fast oscillatory spike bursts have a role in feature extraction will allow studies of the mechanism underlying fast burst discharge to eventually be related to a behavioral function.

The fast oscillations seen in ELL pyramidal cells are very similar to the burst discharge of Layer V pyramidal tract neurons of the cat sensory motor cortex. Calvin termed this type of fast oscillation as an *extra spike mode*. In the extra spike mode large depolarizing afterpotentials immediately following a spike may reach threshold to elicit an extra spike within a few milliseconds, producing the equivalent of a spike doublet (Calvin 1975).

Gray and McCormick (1996) also found that a subset of pyramidal neurons named "chattering cells" in the striate and peristriate cortex generate oscillations in the frequency range of 20 - 70 Hz when depolarized or during visual stimulation. They believe that these fast oscillating cells play a role in recruiting large populations of cells into synchronous firing assemblies. Chattering cells display tonic spike discharge near threshold levels of depolarizing current injection. With increased levels of current injection the cell shifts from a tonic to burst discharge of 20 - 70 Hz which may also be seen in response to

optimal visual stimuli. Chattering cells also typically fire burst discharge when the ISI reaches ~ 3 ms (Gray and McCormick, 1996). This resembles the frequency dependence of burst discharge in ELL pyramidal cells which may generate bursts once spike discharge reaches an ISI of 3 – 8 ms.

Moreover, Xiao-Jing Wang (1999) has created a model of chattering cells based on the basic mechanism of bursting described for ELL cells by Turner et al. (1994) which involves spike backpropagation. Both the ELL pyramidal cell and "chattering cells" have a pronounced fAHP and DAP and both typically fire in bursts of 2 - 5 spikes. There are however differences between the output of chattering cells in Wang's model and the output of the pyramidal cells in the ELL. When a burst terminates in Wang's model it is followed by a subthreshold DAP not seen in our pyramidal cells. In Wang's model, increased current injection to the chattering cell eventually changes output from bursting to rapid tonic firing. The opposite effect is seen with pyramidal cells of the ELL where the cell maintains burst discharge once it is initiated.

In recent years the physiological role of fast oscillatory discharge has become increasingly apparent. Wang's model (1999) showed that burst discharge by a "chattering cell" was required for the rythmycity to be reliably transmitted to the postsynaptic cell via unreliable synapses. Wang (1998) also shows in his model that fast burst firing of chattering neurons provides an exceptionally powerful drive in recruiting feed back inhibition in cortical circuits. High frequency burst firing provides more precise information than action potentials that arrive singly for hippocampal CA1 synapses (Lisman, 1997), and bursts generated by visual stimulation in the lateral geniculate nucleus enhance the detection of dim stimuli (Mukherjee and Kaplan, 1995, Guido, et al. 1995). Finally, burst fir-

ing patterns have a direct relation to behavior (Calvin & Loeser, 1975), states of consciousness (Steriade et al, 1993), and the secretion of vassopressin in magnocellular neuroendocrine cells (Andrew & Dudek, 1983).

FUNCTIONAL SIGNIFICANCE OF SPIKE BACKPROPAGATION

Many neurons initiate Na^+ spike discharge near the soma which is followed by spike backpropagation over extensive regions of the dendritic arbor (Turner et al., 1991; Jaffe et al., 1992; Spruston et al., 1995; Colbert and Johnston, 1996; Johnston et al., 1996; Larkum et al., 1996; Chen et al., 1997; Stuart et al., 1997). Recent work has begun to identify the functional significance of backpropagating spikes, including a role in synaptic plasticity, enhancing dendrite-soma coupling, and presynaptic transmitter release (Spruston et al., 1995; Callaway and Ross 1995; Markram et al., 1997; Bischofberger and Jones, 1997; Chen et al., 1997; Magee and Johnston, 1997; Magee et al., 1998; Larkum et al., 1999). This work on ELL pyramidal cells establishes a key role for a conditional backpropagation of spikes in generating oscillatory burst discharge that will likely extend to many different cell types (Zhang et al., 1993; Paré et al., 1995; Mainen and Sejnowski, 1996; Wang, 1999).

Spike bursts in cortical cells have become recognized for their role in encoding stimulus location, orientation, and spatial frequency selectivity (Lisman, 1997). Similarly, burst discharge in ELL pyramidal cells *in vivo* has a direct role in feature extraction (Gabbiani et al., 1996; Metzner et al., 1998). An intriguing feature of the ELL is the presence of multiple topographic maps of electroreceptor distribution (Maler et al., 1991). Pyramidal cells in each of these maps contribute to specific behaviours (Metzner and Juranek, 1997) and exhibit a frequency selectivity *in vivo* that varies in concert with oscil-

latory properties *in vitro* (Shumway et al., 1989; Turner et al., 1996). The distribution or kinetics of ion channels that control burst output may then regulate pyramidal cell output between sensory maps, emphasizing the potential for dendritic ion channels to modulate sensory processing.

REFERENCES

Akusa, T., Nishimura, T., and Tokimasa, T. (1990) Calcium-dependent chloride current in neurons of the rabbit pelvic parsympathetic ganglia. *Journal of Physiology, London* 422:303-320.

Aldrich, R.W., Getting, P.A., and Thomson, S.H. (1979) Mechanism of frequency-dependent broadening of molluscan neuron soma spikes. *Journal of Physiology, London* 291:531-544.

Andrew, David R. & Dudek, Edward F. (1983) Burst discharge in mammalian neuroendocrine cells involves an intrinsic regenerative mechanism. *Science* 221:1050-1052.

Assad, C., Rasnow, B., Stoddard P.K., and Bower J.M. (1998) The electric organ discharges of the gymnotiform fishes: II. Eigenmannia. *Journal of Comparative Physiology A-Sensory Neural and Behavioral Physiology*183:419-32.

Azouz, R., Jensen, M.S., and Yaari, Y. (1996) Ionic basis of spike after-depolarization and burst generation in adult rat hippocampal CA1 pyramidal cells. *Journal of Physiology, London* 492:211-223.

Bastian, J. (1994) Electrosensory Organisms. *Physics Today* 2:30-37.

Bastian, J., and Courtright, J. (1991) Morphological correlates of pyramidal cell adaptation rate in the electrosensory lateral line lobe of weakly electric fish. *Journal of Comparative Physiology* 168:393-407.

Berman, N.J., and Maler, L. (1998) Interaction of $GABA_B$-mediated inhibition with voltage-gated currents of pyramidal cells: computational mechanism of a sensory searchlight. *Journal of Neurophysiology* 80:3197-3213.

Berman, N.J., and Maler, L. (1998) Inhibition evoked from primary afferents in the electrosensory lateral line lobe of the weakly electric fish (*Apteronotus leptorhynchus*). *Journal of Neurophysiology* 80:3173-3196.

Bischofberger, J., and Jones, P. (1997) Action potential propagation into the presynaptic dendrites of rat mitral cells. *Journal of Physiology, London* 504:359-365.

Borst, J.G.G., and Sakmann, B. (1999) Facilitation of presynaptic calcium currents in the rat brainstem. *Journal of Physiology, London* 513:149-155.

Bourque, C.W., and Renaud, L.P. (1985) Activity dependence of action potential duration in rat supraoptic neurosecretory neurons recorded *in vitro*. *Journal of Physiology, London* 363:429-439.

Bourque, C.W. (1991) Activity-dependent modulation of nerve terminal excitation in a mammalian peptidergic system. *Trends in Neuroscience* 14:28-30.

Bourque, C.W. (1986) Calcium-dependent spike after-current induces burst firing in magnocellular neurosecretory cells. *Neuroscience Letters* 70:204-209.

Bourque, C.W., Randle, J.C.R. and Renaud, L.P. (1986) Non-synaptic depolarizing potentials in rat supraoptic neurones recorded *in vitro*. *Journal of Physiology, London* 376:493-505.

Brew, H. M., and Forsythe, I. D. (1995). Two voltage-dependent K+ conductances with complementary functions in postsynaptic integration at a central auditory synapse. *Journal of Neuroscience* 15:8011-8022.

Buzsaki, G., Penttonen, M., Nadasdy, Z., and Bragin, A. (1996) Pattern and inhibition-dependent invasion of pyramidal cell dendrites by fast spikes in the hippocampus *in vivo*. *Proceedings of the National Academy of Science* 93:9921-9925.

Callaway, J.C, and Ross, W.N. (1995) Frequency-dependent propagation of sodium action potentials in dendrites of hippocampal CA1 pyramidal neurons. *Journal of Neurophysiology* 74:1395-1403.

Calvin, W. H. (1975) Generation of spike trains in CNS neurons. *Brain Research* 84:1-22.

Calvin W.H., and Hartline, D.K. (1977) Retrograde invasion of Lobster stretch receptor somata in control of firing rate and extra spike patterning. *Journal of Neurophysiology* 40:106-118.

Calvin, W. H., and Loeser, J.D. (1975) Doublet and burst firing patterns within the dorsal column nuclei of cat and man. *Experimental Neurology* 48: 406-426.

Calvin W.H., and Sypert, G.W. (1976) Fast and slow pyramidal tract neurons: an intracellular analysis of their contrasting repetitive firing properties in the cat. *Journal of Neurophysiology* 39:420-434.

Carruth, M., Anand, R., and Magee, J.C. (1999) Dendritic K+ channels regulate the firing mode of hippocampal CA1 pyramidal neurons. *Society for Neuroscience Abstract* 25:691.12.

Chen, W.R., Mitgaard, J., and Shepherd, G.M. (1997) Forward and backward propagation of dendritic impulses and their synaptic control in mitral cells. *Science* 278:463-467.

Colbert, C.M., and Johnston, D. (1996) Axonal action-potential initiation and Na^+ channel densities in the soma and axon initial segment of subicular pyramidal neurons. *Journal of Neuroscience* 16:6676-6686.

Colbert, C.M., Magee, J.C., Hoffman, D.A., and Johnston, D. (1997) Slow recovery from inactivation of Na^+ channels underlies the activity-dependent attenuation of dendritic action potentials in hippocampal CA1 pyramidal neurons. *Journal of Neuroscience* 17:6512-6521.

Crunelli, V., Lightowler, S., and Pollard, C.E. (1989) A T-type Ca^{2+}-current underlies low-threshold Ca^{2+} potentials in cells of the cat and rat lateral geniculate nucleus. *Journal of Physiology, London* 413:543-561.

Dryer, S.E. (1994) Na^+-activated K^+ channels: a new family of large conductance ion channels. *Trends in Neuroscience* 17:155-160.

Eeckman, F.H., and Freeman, W.J. (1990) Correlations between unit firing and EEG in the rat olfactory system. *Brain Research* 528:238-244.

Fleidervish, I.A., Friedman, A., and Gutnick, M.J. (1996) Slow inactivation of Na^+ current and slow cumulative spike adaptation in mouse and guinea-pig neocortical neurones in slices. *Journal of Physiology, London* 493:83-97.

Gabbiani F, Metzner W, Wessel R, Koch C (1996) From stimulus encoding to feature extraction in weakly electric fish. *Nature* 384:564-567.

Goh, J.W., and Pennefather, P.S. (1987) Pharmacological and physiological properties of the after-hyperpolarization current of bullfrog ganglion neurones. *Journal of Physiology* 394: 315-330.

Golding, N.L., Jung, H-Y., Mickus, T., and Spruston, N. (1999) Dendritic calcium spike initiation and repolarization are controlled by distinct potassium channel subtypes in CA1 pyramidal neurons. *Journal of Neuroscience* 19:8789-8798.

Granit, R., Kernell, D., and Smith, R.S. (1963) Delayed depolarization and the repetitive response to intracellular stimulation of mammalian motoneurones. *Journal of Physiology, London* 168:890-910.

Gray, C.M., and McCormick, D. (1996) Chattering cells: superficial pyramidal neurons contributing to the generation of synchronous oscillations in the visual cortex. *Science* 274:109-113.

Guido, W., Lu, S.M., Vaughan, J.W., Godwin, D.W., and Sherman, S.M. (1995) Reciever operating characteristic (ROC) analysis of neurons in the cat's lateral geniculate nucleus during tonic and burst response mode. *Visual Neuroscience*12:723-741.

Halvorsrud, R., Shao, L.R., Bouskila, Y., Ramakers, G.M.J., Borg-Graham, L. and Storm, J.F. (1999) Evidence that BK–type Ca^{2+}-dependent K^{+} channels contribute to frequency-dependent action potential broadening in rat CA1 hippocampal pyramidal cells. *Society for Neuroscience Abstract* 25:179.3.

Heiligenberg, W. (1991) Neural Nets in Electric Fish. *MIT Press*, Cambridge, MA.

Hernández-Pineda, R., Chow, A., Amarillo, Y., Moreno, H., Saganich, M., Vega-Saenz de Miera, E., Hernández-Cruz, A., and Rudy, B. (1999) Kv3.1-Kv3.2 channels underlie a high voltage-activating component of the delayed rectifier K+ current in projecting neurons from globus pallidus. *Journal of Neurophysiology* 82:1512-1528.

Hoehn, K., Watson, T.W.J., and MacVicar, B.A. (1993) A novel tetrodotoxin-insensitive, slow sodium current in striatal and hippocampal neurons. *Neuron* 10:543-552.

Hoffman, D.A., and Johnston, D. (1998) Downregulation of transient K+ channels in dendrites of hippocampal CA1 pyramidal neurons by activation of PKA and PKC. *Journal of Neuroscience* 18:3521-3528.

Hoffman, D.A., and Johnston, D. (1999) Neuromodulation of dendritic action potentials. *Journal of Physiology, London* 22:408-411.

Hoffman, D.A., Magee, J.C., Colbert, C.M. and Johnston, D. (1997) K+ channel regulation of signal propagation in dendrites of hippocampal pyramidal neurons. *Nature* 387:869-875.

Hotson, J.R., and Prince, D.A. (1980) A calcium activated hyperpolarization follows repetitive firing in hippocampal neurons. *Journal of Neurophysiology* 43(2):409-419.

Huguenard, J.R. (1996) Low-threshold calcium currents in central nervous system neurons. *Annual Review of Physiology* 58:329-48.

Jackson, M.B., Konnerth, A., and Augustine, G.J. (1991) Action potential broadening and frequency-dependent facilitation of calcium signals in pituitary nerve terminals. *Proceedings National Academy of Science* 88:380-384.

Jaffe D.B., Johnston, D., Lasser-Ross N., Lisman, E., Miyakawa, H., and Ross, W.N. (1992) The spread of Na^{+} spikes determines the pattern of dendritic Ca^{2+} entry into hippocampal neurons. *Nature* 357:244-246.

Jefferys, J.G.R., Traub, R.D., and Whittington, M.A. (1996) Neuronal networks for induced "40 Hz" rhythms. *Trends in Neuroscience* 19:202-208.

Johnston, D., Magee. J.C., Colbert, C.M., and Christie, B.R. (1996) Active properties of neuronal dendrites. *Annual Review of Neuroscience* 19:165-186.

Johnston, D., Hablitz, J.J., and Wilson, W.A. (1980) Voltage clamp discloses slow inward current in hippocampal burst-firing neurones. *Nature* 286:391-393.

Joho, R.J., Chi, S.H., and Marks, G.A. (1999) Increased γ- and decreased δ-oscillations in a mouse deficient for a potassium channel expressed in fast-spiking interneurons. *Journal of Neurophysiology* 82:1855-1864.

Jung., H., Staff, N., and Spruston, N. (1999) Ionic basis of intrinsic bursting in rat subicular neurons. *Society for Neuroscience Abstract* 25:691.10.

Kang, Y., and Ohmori, H. (1999) Depolarizing afterpotentials involved in generation of burst firing in cortical pyramidal cells *in vitro*. *Society for Neuroscience Abstract* 25:664.13.

Kanemasa, T., Gan, L., Perney, T.M., Wang, L-Y., and Kaczmarek, L.K. (1995) Electrophysiological and pharmacological characterization of a mammalian Shaw channel expressed in NIH 3T3 fibroblasts. *Journal of Neurophysiology* 74:207-217.

Klemic, K.G., Shieh, C-C., Kirsch, G.E., and Jones, S.W. (1998) Inactivation of Kv2.1 potassium channels. *Biophysical Journal* 74:1779-1789.

Koch, C. (1999) Biophysics of computation. New York: Oxford University Press.

Kotecha, S., Eley, D.W., and Turner R.W. (1997) Tissue printed cells from teleost electrosensory and cerebellar structures. *Journal of Comparative Neurology* 386:277-292.

Larkum, M.E., Rioult, M.G., and Luscher, H-R. (1996) Propagation of action potentials in the dendrites of neurons from rat spinal cord slice cultures. *Journal of Neurophysiology* 75:154-170.

Larkum, M.E., Zhu, J.J., Sakmann, B. (1999) A new cellular mechanism for coupling inputs arriving at different cortical layers. *Nature* 398:338-341.

Lemon, N., Lowe, M., and Turner, R.W. (1998) Factors controlling oscillatory discharge in pyramidal cells of the electrosensory lateral line lobe (ELL) of weakly electric fish. *International Congress of Neuroethology, San Diego Abstract* 343.

Lemon, N., and Turner, R.W. (1999) Backpropagating spikes regulate oscillatory spike bursts. *Society for Neuroscience Abstract* 25:179.12.

Lisman, J.E. (1997) Bursts as a unit of neural information: making unreliable synapses reliable. *TINS* 20:28-43.

Ma, M., and Koester, J. (1995) Consequences and mechanisms of spike broadening of R20 cells in *Aplysia Californica. Journal of Neuroscience* 15:6720-6734.

Magee, J.C. (1998) Dendritic hyperpolarization-activated currents modify the integrative properties of hippocampal CA1 pyramidal neurons. *Journal of Neuroscience* 18:7613-7624.

Magee, J.C., and Carruth, M. (1999) Dendritic voltage-gated ion channels regulate the action potential firing mode of hippocampal CA1 pyramidal neurons. *Journal of Neurophysiology* 82:1895-1901.

Magee, J., Hoffman, D., Colbert C., and Johnston, D. (1998) Electrical and calcium signaling in dendrites of hippocampal pyramidal neurons. *Annual Review of Physiology* 60:327-346.

Magee, J.C., and Johnston, D. (1997) A synaptically controlled, associative signal for Hebbian plasticity in hippocampal neurons. *Science* 275:209-213.

Mainen, Z.F., Joerges, J., Huguenard, J.R., and Sejnowski, T.J. (1995) A model of spike initiation in neocortical pyramidal neurons. *Neuron* 15:1427-1439.

Mainen Z.F., and Sejnowski, T.J. (1996) Influence of dendritic structure on firing pattern in model neocortical neurons. *Nature* 382:363-365.

Maler L (1979) The posterior lateral line lobe of certain gymnotoid fish: Quantitative light microscopy. *Journal of Comparative Neurology* 183:323-363.

Maler, L., Sas, E., Johnston, S.A., and Ellis, W.G. (1991) An atlas of the brain of the electric fish *Apteronotus leptorhynchus. Journal of Chemical Neuroanatomy* 4:1-38.

Maler, L., Sas, E., and Rogers, J. (1981) The cytology of the posterior lateral line lobe of high frequency weakly electric fish (Gymnotidae): Dendritic differentiation and synaptic specificity in a simple cortex. *Journal of Comparative Neurology* 195:87-139.

Markram, H., Lubke, J., Frotscher, M., and Sakmann, B. (1997) Regulation of synaptic efficacy by coincidence of postsynaptic APs and EPSPs. *Science* 275:213-215.

Martina, M., Schultz, J. H., Ehmke, H., Monyer, H., and Jonas, P. (1998) Functional and molecular differences between voltage-gated K+ channels of fast-spiking interneurons and pyramidal neurons of rat hippocampus. *Journal of Neuroscience* 18:8111-8125.

Massengill, J.L., Smith, M.A., Son, D.I., and O'Dowd, D.K. (1997) Differential expression of K4-AP currents and Kv3.1 potassium channel transcripts in cortical neurons that develop distinct firing phenotypes. *Journal of Neuroscience* 17:3136-3147.

Mathes, C., Rosenthal J.J.C., Armstrong, C.M., and Gilly, W.F. (1997) Fast inactivation of delayed rectifier K^+ conductance in squid giant axon and its cell bodies. *Journal General Physiology* 109:435-448.

Mathieson, W.B., and Maler, L. (1988) Morphological and electrophysiological properties of a novel *in vitro* slice preparation: the electrosensory lateral line lobe brain slice. *Journal of Comparative Physiology* 163:489-506.

Mayer, M. (1985) A calcium-activated chloride current generates the after-depolarization of rat sensory neurons in culture. *Journal of Physiology, London* 364:217-239.

McCormick, D., and Huguenard, J.R. (1992) A model of the electrophysiological properties of thalamocortical relay neurons. *Journal of Neurophysiology* 68:1384-1400.

McCormick, D., and Pape, H. (1990) Properties of a hyperpolarization-activated cation current and its role in rhythmic oscillation in thalamic relay neurons. *Journal of Physiology* 431:291-318.

Metzner, W., and Juranek, J. (1997) A sensory brain map for each behavior? *Proceedings of the National Academy of Science* 94:14798-14803.

Metzner, W., Koch, C., Wessel R., and Gabbiani F. (1998) Feature extraction of burst-like spike patterns in multiple sensory maps. *Journal of Neuroscience* 15:2283-2300.

Mickus, T., Jung, H., and Spruston, N. (1999) Properties of slow, cumulative sodium channel inactivation in rat hippocampal CA1 pyramidal neurons. *Biophysical Journal* 76:846-860.

Miyakawa, H., and Kato, H. (1986) Active properties of dendritic membrane examined by current source density analysis in hippocampal CA1 pyramidal neurons. *Brain Research.* 399:303-309.

Moller, P. (1995) Electric Fishes History and Behavior. *Chapman and Hall*, London.

Morales, E., Sinclair, S., and Turner, R.W. (1998) Somatic and dendritic K^+-single channels in pyramidal cells of the electrosensory lobe (ELL) of the weakly electric fish. *International Congress of Neuroethology, San Diego Abstract* 342.

Mukherjee, P., and Kaplan, E. (1995) Dynamics of neurons in the cat lateral geniculate nucleus: *in vivo* electrophysiology and computational modeling. *Journal of Neurophysiology* 74:1222-1243.

Nelson, P.G., and Burke, R.E. (1967) Delayed depolarization in cat spinal motoneurons. *Experimental Neurology* 17:16-26.

Owen, D.G., Segal, M., and Barker J.L. (1986) Voltage-clamp analysis of a Ca^{2+} - and voltage-dependent chloride conductance in cultured mouse spinal neurons. *Journal of Neurophysiology* 55:1115-1135.

Pape, H.C. (1996) Queer current and pacemaker: the hyperpolarization-activated cation current in neurons. *Annual Review of Physiology* 58:299-327.

Pare, D., Pape, H.C., and Dong, J. (1995) Bursting and oscillating neurons of the basolateral amygdaloid complex *in vivo*: electrophysiological properties and morphological features. *Journal of Neurophysiology* 74:1179-1191.

Perney, T. M., and Kaczmarek, L. K. (1997) Localization of a high threshold potassium channel in the rat cochlear nucleus. *Journal of Comparative Neurology* 386:178-202.

Quattrocki, E.A., Marshall, J., and Kaczmarek, L.K. (1994) A Shab potassium channel contributes to action potential broadening in peptidergic neurons. *Neuron* 12:73-86.

Rashid, A.J., and Dunn, R.J. (1998a) A family of Kv3-related K^+ channels in the weakly electric fish *Apteronotus leptorhynchus. International Congress of Neuroethology, San Diego Abstract 341.*

Rashid, A.J., and Dunn, R.J. (1998b) Sequence diversity of voltage-gated potassium channels in an electric fish. *Molecular Brain Research* 54:101-107.

Richardson, T.L., Turner, R.W., and Miller, J.J. (1987) Action potential discharge in hippocampal CA1 pyramidal neurons: current source-density analysis. *Journal of Neurophysiology* 58:981-996.

Scott, R.H., McGuirk, S.M. and Dolphin, A.C. (1988) Modulation of divalent cation-activated chloride ion currents. *British Journal of Pharmacology* 94:653-662.

Shumway CA (1989) Multiple electrosensory maps in the medulla of weakly electric gymnotiform fish. I. Physiological differences. *Journal of Neuroscience* 9:4388-4399.

Sourdet, V., Ferrand, N., and Debanne, D. (1999) Activity-dependent attenuation of action potential backpropagation in rat neocortical dendrites. *Society for Neuroscience Abstract* 25:289.2.

Spruston, N., Schiller, Y., Stuart, G., and Sakmann, B. (1995) Activity-dependent action potential invasion and calcium influx into hippocampal CA1 pyramidal cells. *Science* 268:297-300.

Steriade, M., Curro Dossi, R., and Contreras, D. (1993) Electrophysiological properties of intralaminar thalamocortical cells discharging rhythmic (approximately 40 Hz) spike-bursts at approximately 1000 Hz during waking and rapid eye movement sleep. *Neuroscience* 56:1-9.

Stuart, G.J., and Sakmann, B. (1994) Active propagation of somatic action potentials into neocortical pyramidal cell dendrites. *Nature* 367:69-72.

Stuart, G.J., Shiller, J., and Sakmann, B. (1997) Action potential initiation and propagation in rat neocortical pyramidal neurons. *Journal of Physiology, London* 505:617-632.

Sugita, S., Tanaka, E., and North, R. A. (1993) Membrane properties and synaptic potentials of three types of neurone in rat lateral amygdala. *Journal of Physiology, London* 460:705-718.

Tkatch, T., Baranasauskas, G., and Surmeier, D.J. (1999) Kv3.4 K^+ channels may be responsible for spike broadening during burst firing in globus pallidus neurons. *Society for Neuroscience Abstract* 25:179.17.

Tokimasa, T., Nishimua, T., and Akasu, T. (1988) Calcium-activated chloride conductance in parasympathetic neurons of the rabbit urinary bladder. *Journal of the Autonomic Nervous System* 24:123-131.

Tsubokawa, H., and Ross, W.N. (1996) IPSPs modulate spike backpropagation and associated $[Ca^{2+}]_i$ changes in the dendrites of hippocampal CA1 pyramidal neurons. *Journal of Neurophysiology* 76:2896-2906.

Turner, R.W., Maler, L., Deerinck, T., Levinson R.S., and Ellisman MH (1994) TTX-sensitive dendritic sodium channels underlie oscillatory discharge in a vertebrate sensory neuron. *Journal of Neuroscience* 14:6453-6471.

Turner R.W., Plant J., and Maler, L. (1996) Oscillatory and burst discharge across electrosensory topographic maps. *Journal of Neurophysiology* 76:2364-2382.

Turner R.W., Meyers, D.E.R., Richardson T.L., and Barker J.L. (1991) The site for initiation of action potential discharge over the somato-dendritic axis of rat hippocampal CA1 pyramidal neurons. *Journal of Neuroscience* 11:2270-2280.

Wang, X.J. (1999) Fast burst firing and short-term synaptic plasticity: a model of neocortical chattering neurons. *Neuroscience* 89:347-362.

Whittington, M., Stanford, I., Colling, S., Jefferys, J., and Traub, R. (1997) Spatiotemporal patterns of gamma frequency oscillations tetanically induced in the rat hippocampal slice. *Journal of Physiology, London* 328:621-624.

Yuste, R., and Tank, D.W. (1996) Dendritic integration in mammalian neurons, a century after Cajal. *Neuron* 16:701-716.

Zhang, L., Valiante, T.A., and Carlen, P.L. (1993) Contribution of the low-threshold T-type calcium current in generating the post-spike depolarizing afterpotential in dentate granule neurons of immature rats. *Journal of Neurophysiology* 70:1-9.